The degree of the recovery is variable and may be dependent on several factors, including the protocol of MPTP treatment, the species, and the method of behavioral evaluation. Interestingly, the functional recovery observed in medaka was not accompanied by the restoration of the number of $TH^+$ cells or by increase in the amount of dopamine to a normal level in the adult stage. The striatum of MPTP-treated medaka did not show robust denervation of the $TH^+$ neurons, and this may explain the behavioral recovery observed in our medaka. Such complete behavioral recovery despite the incomplete return of the amount of dopamine may take place as in squirrel monkeys, possibly due to alteration in dopamine metabolism and neuronal sprouting (Petzinger et al., 2006).

In summary we have generated a medaka PD model by treating larval fish with MPTP, and established reliable assays from the larval stage to the adult. Our protocol of inducing PD-like phenotypes and our assay described in this study provides invaluable tools to investigate medaka model of familial PD retrieved from the TILLING library or medaka treated by other toxins or drugs.

## Acknowledgements

We are grateful to all the technical staff of the Department of Radiation Genetics and all the people of the Department of Neurology.

## Appendix A. Supplementary data

Supplementary data associated with this article can be found, in the online version, at doi:10.1016/j.neures.2009.07.010.

## References

Aida, T., 1921. On the inheritance of color in a fresh-water fish, *Aplocheilus latipes* Temminck and Schlegel, with special reference to sex-linked inheritance. Genetics 6, 554–573.

Anichtchik, O.V., Kaslin, J., Peitsaro, N., Scheinin, M., Panula, P., 2004. Neurochemical and behavioral changes in zebrafish *Danio rerio* after systemic administration of 6-hydroxydopamine and 1-methyl-4-phenyl-1,2,3,6-tetrahydropyridine. J. Neurochem. 88, 443–453.

Bonifati, V., Rizzu, P., van Baren, M.J., Schaap, O., Breedveld, G.J., Krieger, E., Dekker, M.C., Squitieri, F., Ibanez, P., Joosse, M., van Dongen, J.W., Vanacore, N., van Swieten, J.C., Brice, A., Meco, G., van Duijn, C.M., Oostra, B.A., Heutink, P., 2003. Mutations in the DJ-1 gene associated with autosomal recessive early-onset parkinsonism. Science 299, 256–259.

Bové, J., Prou, D., Perier, C., Przedborski, S., 2005. Toxin-induced models of Parkinson's disease. NeuroRx 2, 484–494.

Bretaud, S., Lee, S., Guo, S., 2004. Sensitivity of zebrafish to environmental toxins implicated in Parkinson's disease. Neurotoxicol. Teratol. 26, 857–864.

Cauchi, R.J., van den Heuvel, M., 2006. The fly as a model for neurodegenerative diseases: is it worth the jump? Neurodegener. Dis. 3, 338–356.

Elsworth, J.D., Deutch, A.Y., Redmond Jr., D.E., Sladek Jr., J.R., Roth, R.H., 1990. MPTP-induced parkinsonism: relative changes in dopamine concentration in subregions of substantia nigra, ventral tegmental area and retrorubral field of symptomatic and asymptomatic vervet monkeys. Brain Res. 513, 320–324.

Elsworth, J.D., Taylor, J.R., Sladek Jr., J.R., Collier, T.J., Redmond Jr., D.E., Roth, R.H., 2000. Striatal dopaminergic correlates of stable parkinsonism and degree of recovery in old-world primates one year after MPTP treatment. Neuroscience 95, 399–408.

Fleming, S.M., Fernagut, P.O., Chesselet, M.F., 2005. Genetic mouse models of parkinsonism: strengths and limitations. NeuroRx 2, 495–503.

Gasser, T., 2005. Genetics of Parkinson's disease. Curr. Opin. Neurol. 18, 363–369.

Gerlach, M., Riederer, P., Przuntek, H., Youdim, M.B., 1991. MPTP mechanisms of neurotoxicity and their implications for Parkinson's disease. Eur. J. Pharmacol. 208, 273–286.

Grandel, H., Kaslin, J., Ganz, J., Wenzel, I., Brand, M., 2006. Neural stem cells and neurogenesis in the adult zebrafish brain: origin, proliferation dynamics, migration and cell fate. Dev. Biol. 295, 263–277.

Irwin, I., DeLanney, L.E., Forno, L.S., Finnegan, K.T., Di Monte, D.A., Langston, J.W., 1990. The evolution of nigrostriatal neurochemical changes in the MPTP-treated squirrel monkey. Brain Res. 531, 242–252.

Kapsimali, M., Bourrat, F., Vernier, P., 2001. Distribution of the orphan nuclear receptor Nurr1 in medaka (*Oryzias latipes*): cues to the definition of homologous cell groups in the vertebrate brain. J. Comp. Neurol. 431, 276–292.

Kasahara, M., Naruse, K., Sasaki, S., Nakatani, Y., Qu, W., Ahsan, B., Yamada, T., Nagayasu, Y., Doi, K., Kasai, Y., Jindo, T., Kobayashi, D., Shimada, A., Toyoda, A., Kuroki, Y., Fujiyama, A., Sasaki, T., Shimizu, A., Asakawa, S., Shimizu, N., Hashimoto, S., Yang, J., Lee, Y., Matsushima, K., Sugano, S., Sakaizumi, M., Narita, T., Ohishi, K., Haga, S., Ohta, F., Nomoto, H., Nogata, K., Morishita, T., Endo, T., Shin-I, T., Takeda, H., Morishita, S., Kohara, Y., 2007. The medaka draft genome and insights into vertebrate genome evolution. Nature 447, 714–719.

Kitada, T., Asakawa, S., Hattori, N., Matsumine, H., Yamamura, Y., Minoshima, S., Yokochi, M., Mizuno, Y., Shimizu, N., 1998. Mutations in the parkin gene cause autosomal recessive juvenile parkinsonism. Nature 392, 605–608.

Kurlan, R., Kim, M.H., Gash, D., 1991. The time course and magnitude of spontaneous recovery of parkinsonism produced by intracarotid administration of 1-methyl-4-phenyl-1,2,3,6-tetrahydropyridine to monkeys. Ann. Neurol. 29, 677–679.

Lam, C.S., Korzh, V., Strahle, U., 2005. Zebrafish embryos are susceptible to the dopaminergic neurotoxin MPTP. Eur. J. Neurosci. 21, 1758–1762.

McKinley, E.T., Baranowski, T.C., Blavo, D.O., Cato, C., Doan, T.N., Rubinstein, A.L., 2005. Neuroprotection of MPTP-induced toxicity in zebrafish dopaminergic neurons. Brain Res. Mol. Brain Res. 141, 128–137.

Outeiro, T.F., Lindquist, S., 2003. Yeast cells provide insight into alpha-synuclein biology and pathobiology. Science 302, 1772–1775.

Paisán-Ruíz, C., Jain, S., Evans, E.W., Gilks, W.P., Simón, J., van der Brug, M., López de Munain, A., Aparicio, S., Gil, A.M., Khan, N., Johnson, J., Martinez, J.R., Nicholl, D., Carrera, I.M., Pena, A.S., de Silva, R., Lees, A., Martí-Massó, J.F., Pérez-Tur, J., Wood, N.W., Singleton, A.B., 2004. Cloning of the gene containing mutations that cause PARK8-linked Parkinson's disease. Neuron 44, 595–600.

Petzinger, G.M., Fisher, B., Hogg, E., Abernathy, A., Arevalo, P., Nixon, K., Jakowec, M.W., 2006. Behavioral motor recovery in the 1-methyl-4-phenyl-1,2,3,6-tetrahydropyridine-lesioned squirrel monkey (*Saimiri sciureus*): changes in striatal dopamine and expression of tyrosine hydroxylase and dopamine transporter proteins. J. Neurosci. Res. 83, 332–347.

Pollard, H.B., Dhariwal, K., Adeyemo, O.M., Markey, C.J., Caohuy, H., Levine, M., Markey, S., Youdim, M.B., 1992. A parkinsonian syndrome induced in the goldfish by the neurotoxin MPTP. FASEB J. 6, 3108–3116.

Polymeropoulos, M.H., Lavedan, C., Leroy, E., Ide, S.E., Dehejia, A., Dutra, A., Pike, B., Root, H., Rubenstein, J., Boyer, R., Stenroos, E.S., Chandrasekharappa, S., Athanassiadou, A., Papapetropoulos, T., Johnson, W.G., Lazzarini, A.M., Duvoisin, R.C., Di Iorio, G., Golbe, L.I., Nussbaum, R.L., 1997. Mutation in the alpha-synuclein gene identified in families with Parkinson's disease. Science 276, 2045–2047.

Rink, E., Wullimann, M.F., 2004. Connections of the ventral telencephalon (subpallium) in the zebrafish (*Danio rerio*). Brain Res. 1011, 206–220.

Rogaeva, E., Johnson, J., Lang, A.E., Gulick, C., Gwinn-Hardy, K., Kawarai, T., Sato, C., Morgan, A., Werner, J., Nussbaum, R., Petit, A., Okun, M.S., McInerney, A., Mandel, R., Groen, J.L., Fernandez, H.H., Postuma, R., Foote, K.D., Salehi-Rad, S., Liang, Y., Reimsnider, S., Tandon, A., Hardy, J., St George-Hyslop, P., Singleton, A.B., 2004. Analysis of the PINK1 gene in a large cohort of cases with Parkinson disease. Arch. Neurol. 61, 1898–1904.

Rose, S., Nomoto, M., Jenner, P., Marsden, C.D., 1989. Transient depletion of nucleus accumbens dopamine content may contribute to initial akinesia induced by MPTP in common marmosets. Biochem. Pharmacol. 38, 3677–3681.

Sallinen, V., Torkko, V., Sundvik, M., Reenilä, I., Khrustalyov, D., Kaslin, J., Panula, P., 2009. MPTP and MPP+ target specific aminergic cell populations in larval zebrafish. J. Neurochem. 108, 719–731.

Shimamura, K., Takeichi, M., 1992. Local and transient expression of E-cadherin involved in mouse embryonic brain morphogenesis. Development 116, 1011–1019.

Taniguchi, Y., Takeda, S., Furutani-Seiki, M., Kamei, Y., Todo, T., Sasado, T., Deguchi, T., Kondoh, H., Mudde, J., Yamazoe, M., Hidaka, M., Mitani, H., Toyoda, A., Sakaki, Y., Plasterk, R.H., Cuppen, E., 2006. Generation of medaka gene knockout models by target-selected mutagenesis. Genome Biol. 7, R116.

Valente, E.M., Abou-Sleiman, P.M., Caputo, V., Muqit, M.M., Harvey, K., Gispert, S., Ali, Z., Del Turco, D., Bentivoglio, A.R., Healy, D.G., Albanese, A., Nussbaum, R., González-Maldonado, R., Deller, T., Salvi, S., Cortelli, P., Gilks, W.P., Latchman, D.S., Harvey, R.J., Dallapiccola, B., Auburger, G., Wood, N.W., 2004. Hereditary early-onset Parkinson's disease caused by mutations in PINK1. Science 304, 1158–1160.

van Ham, T.J., Thijssen, K.L., Breitling, R., Hofstra, R.M., Plasterk, R.H., Nollen, E.A., 2008. *C. elegans* model identifies genetic modifiers of alpha-synuclein inclusion formation during aging. PLoS Genet. 4, e1000027.

Wen, L., Wei, W., Gu, W., Huang, P., Ren, X., Zhang, Z., Zhu, Z., Lin, S., Zhang, B., 2008. Visualization of monoaminergic neurons and neurotoxicity of MPTP in live transgenic zebrafish. Dev. Biol. 314, 84–92.

Wittbrodt, J., Shima, A., Schartl, M., 2002. Medaka—a model organism from the far east. Nat. Rev. Genet. 3, 53–64.

Yang, H., Tiersch, T.R., 2009. Current status of sperm cryopreservation in biomedical research fish models: zebrafish, medaka, and Xiphophorus. Comp. Biochem. Physiol. C: Toxicol. Pharmacol. 149, 224–232.

Zimprich, A., Biskup, S., Leitner, P., Lichtner, P., Farrer, M., Lincoln, S., Kachergus, J., Hulihan, M., Uitti, R.J., Calne, D.B., Stoessl, A.J., Pfeiffer, R.F., Patenge, N., Carbajal, I.C., Vieregge, P., Asmus, F., Müller-Myhsok, B., Dickson, D.W., Meitinger, T., Strom, T.M., Wszolek, Z.K., Gasser, T., 2004. Mutations in LRRK2 cause autosomal-dominant parkinsonism with pleomorphic pathology. Neuron 44, 601–607.

Zupanc, G.K., 2008. Adult neurogenesis and neuronal regeneration in the brain of teleost fish. J. Physiol. Paris 102, 357–373.

Clinical Neurophysiology 120 (2009) 1923–1926

Contents lists available at ScienceDirect

Clinical Neurophysiology

journal homepage: www.elsevier.com/locate/clinph

# Abnormal auditory cortex with giant N100m signal in patients with autosomal dominant lateral temporal lobe epilepsy

Keiko Usui [a,d], Akio Ikeda [b,*], Takashi Nagamine [a], Jun Matsubayashi [a], Riki Matsumoto [b], Harukazu Hiraumi [c], Jun Kawamata [b], Masao Matsuhashi [a], Ryosuke Takahashi [b], Hidenao Fukuyama [a]

[a] Human Brain Research Center, Kyoto University Graduate School of Medicine, Kyoto, Japan
[b] Department of Neurology, Kyoto University Graduate School of Medicine, Kyoto, Japan
[c] Department of Otolaryngology, Head and Neck Surgery, Kyoto University Graduate School of Medicine, Kyoto, Japan
[d] National Epilepsy Center, Shizuoka Institute of Epilepsy and Neurological Disorders, Shizuoka, Japan

ARTICLE INFO

*Article history:*
Accepted 24 August 2009
Available online 29 September 2009

*Keywords:*
Auditory evoked magnetic fields (AEF)
MEG
Auditory aura
ADLTE
Cortical hyperexcitability

ABSTRACT

*Objective:* Lateralization of functionally abnormal cortical area in autosomal dominant lateral temporal lobe epilepsy (ADLTE).
*Methods:* A sound pulse of pure tone was delivered monaurally to the ears alternately. Auditory evoked magnetic fields (AEF) were measured by using whole-head magnetoencephalography (MEG) system.
*Results:* Significantly large N100m signals (a magnetic counterpart of N1/N100 in EEG) were detected in three out of five patients, either in the left or in the right hemisphere, contralateral to the auditory stimulation. The peak latency, location and orientation of distinct N100m exhibited no clear difference from those of normal controls.
*Conclusions:* Unilateral cortical abnormality exists in some of the patients in ADLTE. Patients with abnormally large N100m had seizures apparently provoked by auditory stimuli, suggesting that the appearance of significantly large N100m is associated with the epileptogenicity. Based on the detailed examination using MRI and FDG-PET for two of the patients, the authors hypothesize hyperexcitability caused by the decreased inhibitory functions, larger number of synchronously activated neurons, or the elongation of neuronal firing in the pathological temporal cortex in ADLTE.
*Significance:* The present study revealed clear abnormalities in the auditory cortex that have not been well detected by conventional EEG in patients with ADLTE.
© 2009 International Federation of Clinical Neurophysiology. Published by Elsevier Ireland Ltd. All rights reserved.

## 1. Introduction

Direct evidence that the seizures originate from a specific region is obtained only when epileptic cortical activities are recorded in that particular region. Epileptic seizures usually occur sporadically and, in most cases, little neurological deficit is found during the interictal period. EEG is useful to find the abnormal cortical activities during seizures. In the interictal period, however, abnormal activities are sometimes not found in EEG. Evoked potentials (EPs) have been used to evaluate abnormality in various neurological diseases. In epileptic syndromes, it is known that somatosensory evoked potentials (SEPs) or their magnetic counterparts are extremely large in patients with progressive myoclonic epilepsy (Dawson, 1946; Watson and Denny-Brown, 1955; Halliday, 1967; Chadwick et al., 1977; Shibasaki et al., 1978; Hallett et al., 1979; Karhu et al., 1994). In other types of epilepsy, however, EPs have rarely been used to investigate latent cortical abnormality.

Autosomal dominant lateral temporal lobe epilepsy (ADLTE) is one of the rare genetic epilepsies that exhibit partial seizures (Ottman et al., 1995; Ikeda et al., 2000, 2007; Michelucci et al., 2003). Since ADLTE is characterized by recurrent auditory auras, it is assumed that the seizure onset or the irritative zone is on the lateral temporal lobe, and that the auditory cortex or its association areas are involved in the epileptic activities. Functionally abnormal cortical area, however, has not yet been clearly localized due to the fact that ictal EEG is scarcely recorded in the cases of ADLTE, and that interictal abnormality observed in EEG is also rare (Ikeda et al., 2000, 2007; Michelucci et al., 2003).

In the present study, we employed evoked magnetic field (AEF) measured by using magnetoencephalography (MEG), a magnetic version of evoked potential technique, for the investigation of interictal abnormality in the cortex in ADLTE. We investigated interictal abnormality in the cortex in ADLTE. MEG picks up

* Corresponding author. Address: Department of Neurology, Kyoto University Graduate School of Medicine, Shogoin, Sakyo-ku, Kyoto 606-8507, Japan. Tel.: +81 75 751 3772; fax: +81 75 751 9416.
*E-mail address:* akio@kuhp.kyoto-u.ac.jp (A. Ikeda).

1388-2457/$36.00 © 2009 International Federation of Clinical Neurophysiology. Published by Elsevier Ireland Ltd. All rights reserved.
doi:10.1016/j.clinph.2009.08.020

cortical activities right beneath the magnetic sensors with high spatial and temporal resolutions, and thus enabled us to evaluate the cortical function of the left and right temporal lobes separately (Hari, 1990). The content of this paper did not appear elsewhere except for an abstract (Ikeda et al., 2007)

### 1.1. Subjects and methods

#### 1.1.1. Subjects

Five right-handed patients from three families with ADLTE participated in the present study. Table 1 shows their clinical profile. The clinical details of the patients, have been reported elsewhere (Ikeda et al., 2000, 2007; Kawamata et al., in press; Fujita et al., 2009). Families U and O were genetically diagnosed as ADLTE (Ikeda et al., 2007; Kawamata et al., in press; Fujita et al., 2009). All patients had auditory auras and three of them (Patients 2, 4 and 5) had seizures triggered by specific sound. In interictal period, no neurological deficits and hearing disturbance were observed. In all patient EEG showed no definite epileptic discharges in interictal period.

3-Tesla or 1.5-Tesla MR images were taken in all patients. MRI showed volume reduction in unilateral temporal lobe in two patients (Patients 4 and 5) and the left hippocampal sclerosis in one patient (Patient 3). [F-18]fluorodeoxyglucose-positron emission tomography (FDG-PET) showed glucose-hypometabolism in the same temporal lobes with MRI abnormality in Patients 3, 4 and 5.

Ten healthy volunteers (2 females) of the age between 20 and 43 y.o. (mean (SD), 30.9(6.1)) with no neurological deficits and hearing disturbance were recruited in the study as normal control. All the procedures were approved by Kyoto University Graduate School and Faculty of Medicine, Ethics Committee and written informed consent was obtained from all patients and normal volunteers.

#### 1.1.2. MEG measurement and analysis

AEFs were measured by using a 306-channel whole-head system (VectorView, Elekta Neuromag, Finland). It was confirmed that the patients with ADLTE had no seizures within 12 hours before the AEF recording. No seizure occurred during the recording. A sound pulse of pure tone of 1000 Hz was delivered through ear tubes monaurally to the right and left ears alternately. Level of the sound pulses was controlled so that both patients and normal volunteers were given auditory stimuli at SL (sensation level) of 50 dB above his or her hearing threshold. Output of the sound pulse generator was individually set at SL (sensation level) of 50 dB above the hearing threshold of each subject or normal controls. The duration of the pulse was 130 ms (the rise and fall time of 10 ms each) with 1000 ± 70-ms intervals.

MEG were recorded with bandpass filter of 0.1–330 Hz and with sampling rate of 997 Hz. Epochs for on-line averaging started 100 ms before the onset of each stimuli and terminated 400 ms after the onset. Each stimulus given to the right or left ear were averaged separately. Epochs containing blinks and/or other artifacts were automatically excluded from averaging. More than 100 epochs for each right- and left ear stimulation were averaged in one measurement. Two or three measurements were performed in each subject in order to confirm that auditory magnetic responses were reproduced.

N100m, a magnetic counterpart of N1/N100 in EEG, which is the most prominent component of AEFs (Pantev et al., 1995; Lutkenhoner and Steinstrater, 1998), were analyzed. The activated brain areas were modeled as equivalent current dipoles (ECDs) (Hamalainen et al., 1993). A spherical model, which is made from each subject's anatomical 0.5-Tesla 3-dimensional MR images (Signa, General Electric, USA), was used for describing the conductivity profile of the brain. The ECDs were estimated from at least 27 channels ( = 9 set of sensors), that covered the field pattern of 100 ms component in auditory magnetic fields over each hemisphere. The ECDs with goodness of fit (GOF) more than 80% and confidence volume (CV) less than 1000 $mm^3$ were used for further analysis.

The mean and standard deviation (SD) of ECD moment and peak latency of N100m were obtained from the control subjects. The data of patients and of control group were compared, and the values that surpassed the mean + 2.5 SD of those obtained from control group were regarded as significantly large.

## 2. Results

Fig. 1 shows representative magnetic responses of a patient (Patient 4) to the auditory stimuli given to the left and right ears. Shown in this figure are waveforms in 306 channels (A and D), largest responses detected by planar gradiometer in the contralateral hemisphere to the stimuli (insets of A and D), magnetic field maps and estimated ECDs at 97 ms from stimulus onset in the contralateral hemisphere (B and E), and the ECDs superimposed on the patient's anatomical MR images (C and F). The latency and estimated ECD moment (strength) of N100m peak in each patient are shown in Table 2 in comparison with the mean (SD) of those in normal controls. In all patients, the peak latency of N100m showed no significant difference from those of the control group. The sources of N100m were localized in the temporal plane in each hemisphere of both patients and control subjects, and no significant difference in the location and orientation of sources was identified.

As for the ECD moment, significantly large response was recorded in three patients either in the left (Patients 2 and 4) or in the right (Patient 5) hemisphere, contralateral to the auditory

**Table 1**
Clinical profile of patients with ADLTE.

| Patient | Age | Sex | Family | Types of aura | Seizure types | Inducing factors of seizures | Findings in MRI and/or FDG-PET |
|---|---|---|---|---|---|---|---|
| 1 | 31 | M | U | Auditory, deja vu | SPS, CPS, *n*-GTCS | None | No abnormal findings |
| 2 | 56 | M | U | Auditory | SPS, CPS, *n*-GTCS | Ringing of phone | No abnormal findings |
| 3 | 27 | F | U | Auditory | SPS, CPS, *n*-GTCS | None | Left hippocampus: sclerosis suspected<br>Left temporal lobe: mild hypometabolism suspected |
| 4 | 27 | F | O | Auditory, deja vu | SPS, CPS | Specific sound, conversation | Left superior temporal gyrus: small in volume<br>Left temporal lobe: hypometabolism |
| 5 | 36 | F | H | Auditory, deja vu | SPS, CPS | Specific music | Right inferior horn of lateral ventricle: enlargement<br>Right temporal lobe: hypometabolism |

SPS, simple partial seizures; CPS, complex partial seizures; *n*-GTCS, nocturnal generalized tonic–clonic seizures.

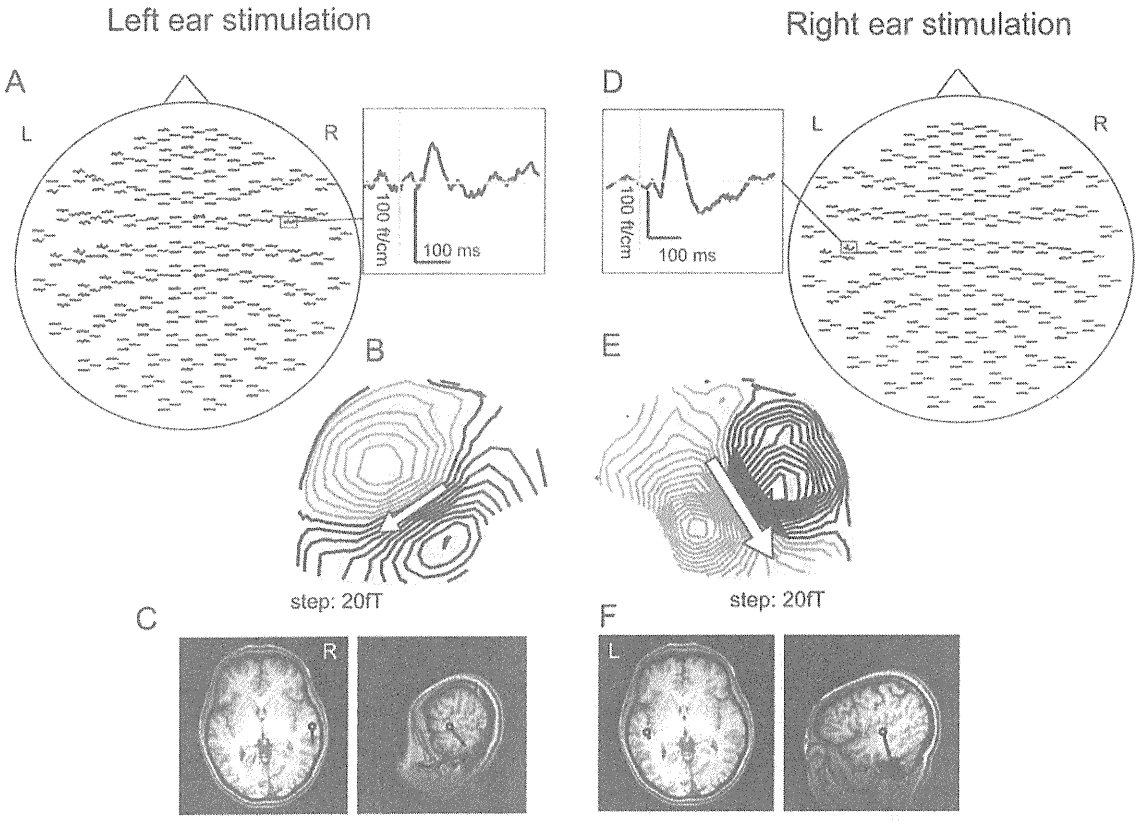


Fig. 1. Auditory evoked magnetic fields of Patient 4. Magnetic responses to the left ear stimulation are shown in the left and the responses to the right ear stimulation in the right. Upper panels (A and D) show responses in all channels. The traces show a 500 ms time period starting 100 ms before the stimulus onset. The insets show the magnified largest responses in the contralateral hemisphere to the stimuli. Lower panels show field map and ECD of N100m. Field patterns in the contralateral hemisphere to the stimuli at the peak latency (97 ms from stimulus onset) are shown in panels (B) and (E). The maps were drawn over the helmet-shaped sensor array. The step between the isocontour lines is 20 fT. The areas with black lines indicate the magnetic field out of the head and the areas with gray lines indicate the field into the head. The arrows show the estimated location of the ECDs projected onto the subject's head surface. Panels (C) and (F) show the ECD location superimposed on the subject's 3-dimensional MR images.

**Table 2**
Peak latency and ECD moment of N100m in the contralateral and ipsilateral hemispheres to unilateral auditory stimuli.

| Subject | Lt ear stimulation | | | | Rt ear stimlation | | | |
|---|---|---|---|---|---|---|---|---|
| | Contralateral (Rt) | | Ipsilateral (Lt) | | Contralateral (Lt) | | Ipsilateral (Rt) | |
| | Latency (ms) | Moment (nAm) | Latency (ms) | Moment (nAm) | Latency (ms) | Moment (nAm) | Latency (ms) | Moment (nAm) |
| P1 | 98 | 40.8 | 112 | 13.0 | 103 | 12.2 | 108 | 27.5 |
| P2 | 106 | 51.2 | 127 | 37.7* | 114 | 88.0* | 114 | 45.5 |
| P3 | 94 | 21.2 | 104 | 13.8 | 98 | 17.7 | 118 | 24.8 |
| P4 | 97 | 18.5 | 96 | 30.6 | 97 | 44.2* | 104 | 13.1 |
| P5 | 97 | 83.7* | 111 | 7.6 | 105 | 15.8 | 114 | 42.3 |
| Control | Latency(SD) | Moment(SD) | Latency(SD) | Moment(SD) | Latency(SD) | Moment(SD) | Latency(SD) | Moment(SD) |
| ($n$ = 10) | 97.3 (5.7) | 35.4 (14.1) | 108.9 (11.8) | 18.5 (6.6) | 98.2 (10.5) | 23.6 (7.3) | 105.7 (8.6) | 27.5 (12.0) |

P, patient; Lt, left; Rt, right. The data of control group are shown as the mean (SD).
* >The mean + 2.5 SD of control group.

stimulation. In the left hemispheres of Patients 2 and 4 and the right hemisphere of Patient 5, large N100m was also evoked in response to the ipsilateral stimuli and the ECD moment was significantly large for Patient 2. In the remaining patients (Patients 1 and 3) the ECD moment of N100m was not different from those of the control group.

## 3. Discussion

Morphological and/or functional abnormality in ADLTE has been reported predominantly on the left hemisphere in the literature so far. In one study, for example, it was reported that morphological abnormality lateralized on the left hemisphere existed in 45% of 22 patients with ADLTE (Kobayashi et al., 2003). Another study reported abnormality in auditory evoked potentials (AEPs) lateralized on the left (Brodtkorb et al., 2005).

Epileptogenicity and functional deficit, however, are caused not only by visually detectable malformations but also by some other abnormalities. In addition, AEP evaluation using EEG and binaural sound presentation are not appropriate to distinguish left and right auditory responses separately. It is, therefore, uncertain how much the causes of ADLTE is associated with morphological abnormality that is localized on the left hemisphere.

In this study using AEF, ECD moment of N100m can be classified into two groups: one with the values larger than +2.5 SD, and the other with the values smaller than +2.5 SD. For brevity, we call the former "large signal" and the latter "small signal". N100m

signals of three patients were clearly larger than those of other patients. The results of these three exhibit unique features that should be mentioned. First noticeable feature is that these larger signals were observed in the left hemisphere for two patients and in the right for the other patient.

Second noticeable and striking feature is that the N100m in the right hemisphere of the two patients who exhibited large signals in the left was small. It is also found that the N100m in the left hemisphere of the other patient who exhibited large signal in the right was small. The fact that the significantly large N100m signals were detected in either left or right hemisphere in three patients, and that the N100m in the opposite hemisphere of all these three patients were small is a clear indication that unilateral cortical abnormality exists, at least in some patients, in ADLTE.

Third noticeable feature is that, as compared with the normal subjects, the latency of large N100m showed no distinct difference in the case of ADLTE patients. This result strongly suggests that no disturbance in both peripheral and central auditory pathways.

Fourth feature is that, although the ECD moment of N100m was distinctively large in the patients, the location and orientation was similar to those in control subjects. The similar location and orientation of the ECD suggested that the center of neuronal populations underlying N100m response are supposed to be the same, or, at least, very close in the giant and normal AEFs. (For detailed mechanism see Eggermont and Ponton, 2002 and references therein)

Further detailed examination for two of the patients using MRI and FDG-PET showed the anatomical and functional deficit localized in the temporal lobes. The volume of the temporal lobe which generated the giant N100m was reduced (possibly due to malformation or atrophy) and glucose-hypometabolism was detected. Volume reduction and hypometabolism usually suggest cortical hypofunction, which is supposed to lead weak signals. The two patients with ADLTE, whose cortical area was reduced in volume, by contrast, generated larger N100m than those with cortices of normal volume.

Since there is no way to reveal the underlying mechanism of the distinctively large ECD moment or the strength of MEG response with concrete experimental evidence in our study so far, we present the hypotheses. One possible explanation is the hyperexcitability of the neurons: the amount of the neurons is the same but the neurons of the patients are hyperreactive. If the neuronal population producing N100m is hyperexcited, the signals would be apparently larger than those of normal activity. Large dipole moment may also indicate highly coordinated activity. If the amount of synchronously activated neurons is larger in the patients with ADLTE than in the normal controls, the signals would be apparently larger. Other possible explanation may be the elongation of neuronal firing. To clearly distinguish the factors affecting the N100m signal, microscopic invasive study using depth or subdural electrodes is needed.

Our investigation found that three patients exhibited distinctively large N100m and the remaining two patients exhibited comparatively small N100m. The difference observed between two groups of patients was that the former had seizures apparently provoked by auditory stimuli, such as specific sound or music, while the latter did not. These facts suggest that the appearance of significantly large N100m in the auditory cortex, which indicates abnormally large response to sound, may be closely associated with the epileptogenicity in these patients, just as giant SEPs in patients with progressive myoclonic epilepsy.

In summary, the present study using auditory magnetic fields showed that significantly large N100m signals are supposed to be an indication of auditory induced seizures. Our result is also a clear demonstration of significant usefulness of AEF in the detailed studies to address the issue of whether unilateral or bilateral temporal lobes are involved. This technique enables these evaluations even for the interictal period.

## Conflict of interest

The authors have no financial conflicts to report.

## Acknowledgement

This study was supported by the Research Grant for The Treatment of Intractable Epilepsy (19-1) from the Japan Ministry of Health, Labor and Welfare, the Scientific Research Grant (C2) (18590935) from the Japan Society for Promotion of Sciences (JSPS) and the Grant-in-Aid for Scientific Research on Priority Areas (20020013) from the Ministry of Education, Culture, Sports, Science and Technology (MEXT).

## References

Brodtkorb E, Steinlein OK, Sand T. Asymmetry of long-latency auditory evoked potentials in LGI1-related autosomal dominant lateral temporal lobe epilepsy. Epilepsia 2005;46:1692–4.

Chadwick D, Hallett M, Harris R, Jenner P, Reynolds EH, Marsden CD. Clinical, biochemical and physiological features distinguishing myoclonus responsive to 5-hydroxytryptophan, tryptophan with a monoamine oxidase inhibitor, and clonazepam. Brain 1977;100:455–87.

Dawson GD. The relation between the electroencephalogram and muscle action potentials in certain convulsive states. J Neurol Neurosurg Psychiatry 1946;10:141–62.

Eggermont JJ, Ponton CW. The neurophysiology of auditory perception: From single units to evoked potentials [review]. Audiol Neurootol 2002;7:71–99.

Fujita Y, Ikeda A, Kadono K, Kawamata J, Tomimoto H, Fukuyama H, Takahashi R. Clinical features in a Japanese patient with autosomal dominant temporal lobe epilepsy having *LGI1* mutation. Clin Neurol (Tokyo) 2009;49:186–90 [in Japanese].

Hallett M, Chadwick D, Marsden CD. Cortical reflex myoclonus. Neurology 1979;29:1107–25.

Halliday AM. The neurophysiological study of myoclonus in man. Brain 1967;90:241–84.

Hamalainen M, Hari R, Ilmoniemi RJ, Knuutila J, Lounasmaa OV. Magnetoencephalography-theory, instrumentation, and applications to noninvasive studies of the working human brain. Rev Modern Phys 1993;65:413–97.

Hari R. The neuromagnetic method in the study of the human auditory cortex. In: Grandori F, Hoke M, Romani G, editors. Auditory evoked magnetic fields and electric potentials. Advances in audiology 1990;vol. 6. Basel: Karger; 1990. p. 222–82.

Ikeda A, Kunieda T, Miyamoto S, Fukuyama H, Shibasaki H. Autosomal dominant temporal lobe epilepsy in a Japanese family. J Neurol Sci 2000;176:162–5.

Ikeda A, Kawamata J, Matsumoto R, Takaya S, Usui K, Fukuyama H, et al. Variable clinical features in Japanese families with autosomal dominant lateral temporal lobe epilepsy (ADLTLE). Neurol Asia 2007;12(Suppl. 1):65 [abstract].

Karhu J, Hari R, Paetau R, Kajola M, Mervaala E. Cortical reactivity in progressive myoclonus epilepsy. Electroencephalogr Clin Neurophysiol 1994;90:93–102.

Kawamata J, Ikeda A, Fujita Y, Usui K, Shimohama S, Takahashi R. Mutation in *LGI1* gene in Japanese Families with autosomal dominant lateral temporal lobe epilepsy: the first report from Asian families. Epilepsia, in press.

Kobayashi E, Santos NF, Torres FR, Secolin R, Sardinha LAC, Lopez-Cendes I, Cendes F. Magnetic resonance imaging abnormalities in familial temporal lobe epilepsy with auditory auras. Arch Neurol 2003;60:1546–51.

Lutkenhoner B, Steinstrater O. High-precision neuromagnetic study of the functional organization of the human auditory cortex. Audiol Neurootol 1998;3:191–213.

Michelucci R, Poza JJ, Sofia V, de Feo MR, Binelli S, Bisulli F, et al. Autosomal dominant lateral temporal epilepsy: clinical spectrum, new epitempin mutations, and genetic heterogeneity in seven European families. Epilepsia 2003;44:1289–97.

Ottman R, Risch N, Hauser WA, Pedley TA, Lee JH, Barker-Cummings C, et al. Localization of a gene for partial epilepsy to chromosome 10q. Nat Genet 1995;10:56–60.

Pantev C, Bertrand O, Eulitz C, Verkindt C, Hampson S, Schiuierer G, Elbert T. Specific tonotopic organizations of different areas of the human auditory cortex revealed by simultaneous magnetic and electric recordings. Electroencephalogr Clin Neurophysiol 1995;94:26–40.

Shibasaki H, Yamashita Y, Kuroiwa Y. Electroencephalographic studies of myoclonus: myoclonus-related cortical spikes and high amplitude somatosensory evoked potentials. Brain 1978;101:447–60.

Watson CW, Denny-Brown D. Studies of the mechanism of stimulus-sensitive myoclonus in man. Electroencephalogr Clin Nueophysiol 1955;7:341–56.

J Neuropathol Exp Neurol
Copyright © 2009 by the American Association of Neuropathologists, Inc.
Vol. 68, No. 10
October 2009
pp. 1084–1091

ORIGINAL ARTICLE

# Selective Nuclear Shrinkage of Oligodendrocytes Lacking Glial Cytoplasmic Inclusions in Multiple System Atrophy: A 3-Dimensional Volumetric Study

Naoto Uyama, MD, Toshiki Uchihara, MD, PhD, Yoko Mochizuki, MD, PhD, Ayako Nakamura, Ryosuke Takahashi, MD, PhD, and Toshio Mizutani, MD, PhD

**Abstract**

Glial cytoplasmic inclusions (GCIs) are a pathologic hallmark of multiple system atrophy (MSA), but their pathogenetic roles need to be clarified. To determine possible roles of GCIs in individual cells, serial optical sections obtained by confocal microscopy were reconstructed to yield 3-dimensional (3D) images of the nuclei to quantify nuclear volume. Oligodendroglial nuclear volumes were determined in the pons of 6 MSA and 7 control patients. The nuclear volumes were significantly smaller in the MSA group as a whole ($135.81 \pm 60.83\ \mu m^3$, mean ± SD; n = 404) than in the control group ($188.05 \pm 55.71\ \mu m^3$; n = 308; $p < 0.001$). This difference was due to a significantly smaller nuclear volume of oligodendrocytes without GCIs ($GCI^-$ group, $91.26 \pm 23.77\ \mu m^3$; n = 210) compared with the control group ($p < 0.001$) and compared with the oligodendrocytes with GCIs ($GCI^+$ group, $184.03 \pm 51.18\ \mu m^3$; n = 194; $p < 0.001$); the difference between the latter $GCI^+$ and control groups was not significant ($p > 0.05$). This selective decrease in nuclear volume restricted to the $GCI^-$ group cannot be explained if nuclear shrinkage was accelerated in the presence of GCIs. Conversely, GCI formation might be linked, either directly or indirectly, to a mechanism that counteracts rather than accelerates nuclear shrinkage. This novel 3-dimensional strategy provides pivotal data that link GCI formation and degeneration in MSA.

**Key Words**: Glial cytoplasmic inclusions, Multiple system atrophy, Nuclear volume, Three-dimensional reconstruction.

From the Department of Neurology (NU, TU, AN), Tokyo Metropolitan Institute for Neuroscience, Tokyo; the Departments of Neurology (NU) and Pathology (YM, TM), Tokyo Metropolitan Neurological Hospital, Tokyo; and the Department of Neurology (NU, RT), Kyoto University, Kyoto, Japan.

Send correspondence and reprint requests to: Toshiki Uchihara, MD, PhD, Department of Neurology, Tokyo Metropolitan Institute for Neuroscience, 2-6 Musashi-dai, Fuchu, Tokyo 183-8526, Japan; E-mail: uchihara-ts@igakuken.or.jp

This study was supported by a research grant from the Tokyo Metropolitan Organization for Medical Research to the Three Dimension Project (Neurology).

Supplemental digital content is available for this article. Direct URL citations appear in the printed text and are provided in the HTML and PDF versions of this article on the journal's Web site (www.jneuropath.com).

## INTRODUCTION

Multiple system atrophy (MSA) (1) is characterized by the distribution of degenerative lesions and the presence of glial cytoplasmic inclusions (GCIs) (2, 3). Because GCIs are a pathologic hallmark of MSA, they are believed to be tightly linked to the pathogenic mechanism of MSA; numerous studies have attempted to clarify possible relationships between the presence of GCIs and the extent and severity of degeneration (4–7). Reported data are, however, highly variable, and none of the previous neuropathologic studies have established a pathogenetic role for GCIs. Although it has been reported that nuclei of GCI-bearing oligodendrocytes ($GCI^+$) usually appear larger than those of oligodendrocytes that do not harbor GCIs ($GCI^-$) (8, 9), it is unclear whether the presence of GCIs is linked to accelerated neurodegeneration. Because the degenerative cascade of MSA leads both to GCI formation and cellular degeneration, the morphologic parameters (e.g. nuclear volume) of an individual oligodendrocyte might be influenced by the formation of GCIs. In this study, we focus on the nuclear volume of oligodendrocytes with or without GCIs. Instead of using conventional indirect methods of volume estimation (10–12), we measured the actual nuclear volume of each oligodendrocyte reconstructed into a 3-dimensional (3D) image from serial optical sections (~200 sections at an interval of 0.1 μm) spanning the entire oligodendrocyte. This straightforward method has been used mainly in the field of diagnostic radiology and provides estimates of the real volume regardless of the shape of the targets (13–15) and is readily applicable to serial data obtained with confocal microscopy (16). This is the first successful attempt to measure directly the actual nuclear volume of oligodendrocytes. Because a decrease in nuclear volume relative to the control was significant only in $GCI^-$ oligodendrocytes but not in $GCI^+$ oligodendrocytes, it is possible to conclude that nuclear shrinkage is accelerated in the absence of GCIs.

## MATERIALS AND METHODS

Six patients with the clinical and neuropathologic diagnosis of MSA (3 men, 3 women; age range at death, 54–74 years) autopsied at the Department of Pathology, Tokyo Metropolitan Neurological Hospital, Tokyo, Japan, and 7 control patients (6 men, 1 women, age range at death, 47–84 years) with no



Copyright © 2009 by the American Association of Neuropathologists, Inc. Unauthorized reproduction of this article is prohibited.

**TABLE 1.** Demographic Features of Patients With MSA and Controls

| Case | Age of Onset/Death, Years | Sex* | Cause of Death | Brain Weight, g |
|---|---|---|---|---|
| MSA 1 | 47/54 | F | Sudden death | 1,310 |
| MSA 2 | 51/58 | M | Pneumonia | 1,318 |
| MSA 3 | 52/59 | F | Pulmonary insufficiency | 1,230 |
| MSA 4 | 57/61 | F | Pulmonary insufficiency | 1,296 |
| MSA 5 | 63/69 | M | Cardiac insufficiency | 1,225 |
| MSA 6 | 70/74 | M | Pulmonary insufficiency | 1,285 |
| Mean ± SD | 56.7 ± 8.5/62.5 ± 7.5† | | | 1,277.3 ± 40.3‡ |
| Control 1 | /47 | M | Guillan-Barré syndrome | 1,390 |
| Control 2 | /67 | F | Thymic anaplastic carcinoma | 1,222 |
| Control 3 | /73 | M | Crow-Fukase syndrome | 1,390 |
| Control 4 | /73 | M | Acute myocardial infarct | 1,320 |
| Control 5 | /81 | M | Chronic constrictive pericarditis | 1,282 |
| Control 6 | /76 | M | CIDP | 1,215 |
| Control 7 | /84 | M | Aortic dissection | 1,225 |
| Mean ± SD | /71.6 ± 12.2 | | | 1,292.0 ± 76.8 |

*No significant difference between control and MSA groups (by Fisher exact test).
†$p > 0.05$ compared with control group (by Student *t*-test).
‡$p > 0.05$ compared with control group (by Student *t*-test).
CIDP, chronic inflammatory demyelinating polyradiculoneuropathy; F, female; M, male; MSA, multiple system atrophy.

disease involving the central nervous system were studied. The durations of MSA ranged from 4 to 7 years (Table 1). The diagnosis of MSA was confirmed postmortem on the basis of neuronal loss and the presence of GCIs in relevant regions, including the putamen, cerebellar white matter, and motor cortex (4). Oligodendrocytes in pontine transverse fibers were chosen for analysis because the size and appearance of oligodendroglial nuclei were relatively homogeneous, which made it easier to quantify and interpret their morphologic changes. Moreover, the high frequency of GCIs in the pons of MSA brains is another advantage in estimating their possible effects.

Formalin-fixed blocks were obtained from the midpons of MSA and control brains, washed in 0.1 mol/L phosphate buffer 3 times, then kept in 15% sucrose/0.1 mol/L phosphate buffer solution until they sank. Free-floating sections 30 μm thick were prepared on a freezing microtome and kept at 4°C until use. These sections were pretreated with 99% formic acid for 5 minutes at room temperature. The sections were blocked with 5% normal goat serum and incubated for 6 days or more at 4°C (17) with a polyclonal rabbit anti-human ubiquitin (Z0458, 1:100, DakoCytomation, Glostrup, Denmark) diluted in 0.01 mol/L PBS containing 0.3% Triton X-100 and 5% normal goat serum. The sections were washed with PBS containing 0.3% Triton X-100 3 times for 10 minutes each between steps of the entire procedure. The sections were then incubated with a polyclonal goat anti-rabbit immunoglobulin G conjugated with Alexa Fluor 546 (1:200; Molecular Probes, Eugene, OR) for 4 hours at room temperature. The sections were then immersed in 0.01 mol/L PBS containing 4′,6-diamidino-2-phenylindole, dihydrochloride (D1306, 1:1500; Molecular Probes) for 5 minutes. After washing, they were mounted with buffered glycerol containing *p*-phenylenediamine to minimize photobleaching. The sections were observed under a fluorescence microscope equipped with a laser confocal system (FV-1000; Olympus, Tokyo, Japan). At least 20 oligodendroglial nuclei from each case were selected randomly by encompassing the entire pontine nucleus; 308 were counted in the control group, 194 in the $GCI^+$ group and 210 in the $GCI^-$ group (Table 2). Oligodendroglial nuclei were identified based on their round and small morphology with a linear alignment in the stretch of 5 to 10 contiguous oligodendrocytes along the long axis of nerve fibers. Larger nuclei of astrocytes or small angular nuclei of microglia (18) (both not in linear alignment) were easily distinguishable. Only cells with round nuclei serially lined in proximity (within twice the diameter of nuclei) along transverse fibers and with comparatively uniform size in the stretches were identified as

**TABLE 2.** Nuclear Volume of Oligodendroglia in MSA and Control Cases

| | Control Cases, n = 7 | Total Oligodendrocytes in MSA Cases, n = 6 | Oligodendrocytes in MSA Cases With GCI | Oligodendrocytes in MSA Cases Without GCI |
|---|---|---|---|---|
| No. oligodendrocytes evaluated | 308 | 404 | 194 | 210 |
| Oligodendrocyte Volume (mean ± SD), $\mu m^3$ | 188.05 ± 55.71 | 135.81 ± 60.83* | 184.03 ± 51.18‡ | 91.26 ± 23.77†§ |

*$p < 0.001$ compared with control group (by Mann-Whitney U test [Bonferroni correction]).
†$p < 0.001$ compared with control group (by 1-way analysis of variance [ANOVA]).
‡No significant difference compared with control group (by 1-way ANOVA).
§$p < 0.001$ compared with $GCI^+$ group (by 1-way ANOVA).
GCI, glial cytoplasmic inclusion; MSA multiple system atrophy.

© 2009 American Association of Neuropathologists, Inc.


Copyright © 2009 by the American Association of Neuropathologists, Inc. Unauthorized reproduction of this article is prohibited.

oligodendrocytes. Serial optical sections at an interval of 0.1 μm were obtained to encompass the entire structure of each oligodendrocyte. Usually, 200 serial optical sections were sufficient to encompass the entire structure of an oligodendrocyte, including GCIs when they were present. Each 3D image data set consisted of a series of 2-dimensional (2D) images (Fig. 1 and Video, Supplemental Digital Content 1, http://links.lww.com/NEN/A60). Each image frame had a 63.5-μm field of view with a 512 × 512-pixel array, yielding 0.124 × 0.124-μm/pixel dimensions. The data were reconstructed for 3D observation and quantification by using software (TRI/3D SRFII-64 Release 4, Ratoc, Tokyo, Japan) running on the Windows platform on a 64-bit basis. To estimate nuclear volume with this software, the 2D contour of each nucleus, along the nuclear membrane labeled with 4′,6-diamidino-2-phenylindole, dihydrochloride, was traced manually on some of the 2D images every 4 to 5 images. The relative position of the manually defined contour and the fluorescence intensity of 4′,6-diamidino-2-phenylindole, dihydrochloride were used to calculate automatically the nuclear contour in intervening optical sections; these were later confirmed by inspection. This yielded the binary representation of the nuclear contour of an oligodendrocyte on a 3D basis consisting of noncubic voxels (0.124 × 0.124 × 0.1 μm). Subsequently, after discarding spurious voxels from the binary oligodendroglial nucleus representation, these data sets were reconstructed for 3D observation and quantification (Video, Supplemental Digital Content 2, http://links.lww.com/NEN/A61), and the total number of voxels, which substitute the nucleus, was obtained on the basis of a known voxel size of 0.0015376 $\mu m^3$, yielding the actual volume size (13–16).

Statistical analyses were performed using Dr. SPSSII for Windows software (SPSS Japan, Tokyo, Japan). Size distributions according to nuclear volume were estimated by the Kolmogorov-Smirnov method to determine whether they were compatible with the normal distribution in each patient or group (control, MSA total [$GCI^+$ and $GCI^-$], $GCI^+$, $GCI^-$). Because the size distribution of the MSA total group did not exhibit normality, its comparison with that of the control group was estimated using the Mann-Whitney U test with Bonferroni correction. Otherwise, the 1-way analysis of variance (ANOVA) was used to compare nuclear volume among the different groups when nuclear sizes exhibited a normal distribution.

## RESULTS

There were no significant differences among groups with respect to age or brain weight (by Student *t*-test) or sex (by Fisher exact test; Table 1). The nuclear volume size distributions are shown in Table 2 and Figures 2 and 3. Because the size distributions showed normal distributions (as determined by the Kolmogorov-Smirnov test when each patient or each group was analyzed), our sampling and volumetric analysis procedure yielded data representative of a homogenous cell group not only in each patient but also in each group. The quantile-quantile plots of data of the $GCI^+$, $GCI^-$, and control groups show almost linear distributions

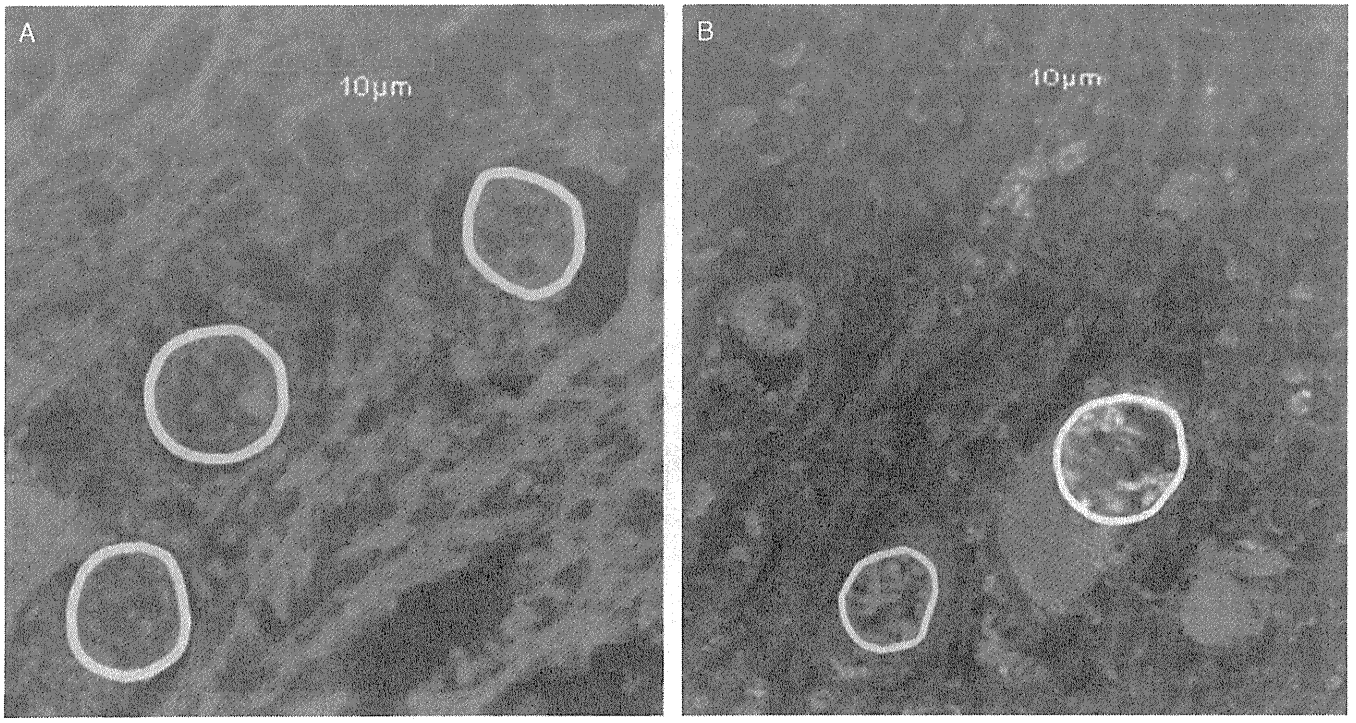


**FIGURE 1.** Pontine oligodendrocytes in control and MSA patients. **(A)** Oligodendrocytes in a control patient. DAPI stain (light blue). **(B)** Oligodendrocytes in an MSA patient. Double-fluorescence labeling for DAPI and ubiquitin (red). The contours of the nucleus of each oligodendrocyte are traced in yellow (oligodendrocytes without glial cytoplasmic inclusions [GCIs]) and in white (oligodendrocyte with GCIs in **B**). Bar = 10 μm. DAPI, 4′,6-diamidino-2-phenylindole, dihydrochloride.


© 2009 American Association of Neuropathologists, Inc.

Copyright © 2009 by the American Association of Neuropathologists, Inc. Unauthorized reproduction of this article is prohibited.

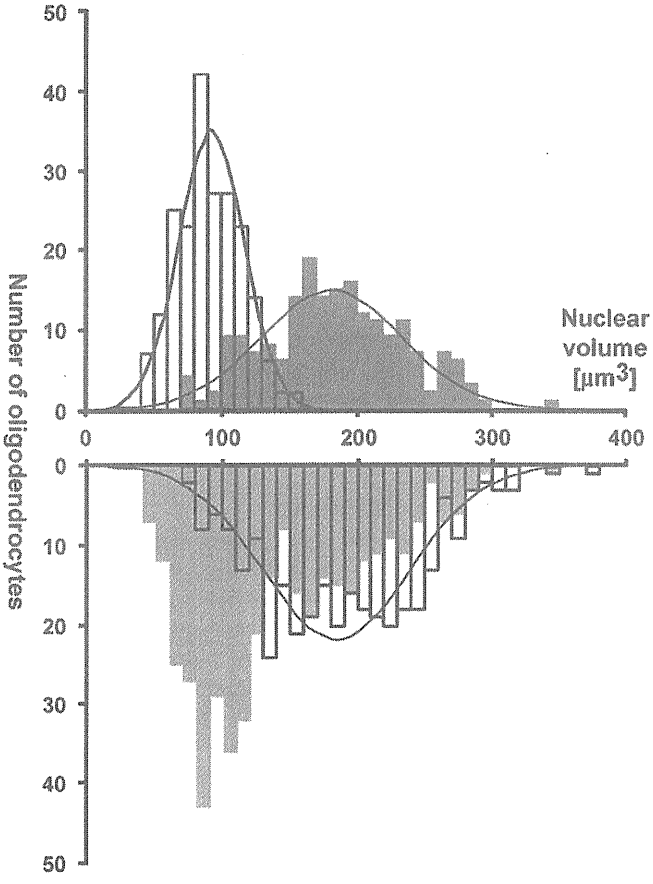


**FIGURE 2.** Histograms of size distribution of oligodendroglial nuclei. The nuclear volumes in cubic microns are expressed on the abscissa. The ordinate represents the relative frequency of calculated nuclear size. The lower inverted histograms represent the controls (unfilled bars with black lines) and the multiple system atrophy (MSA) group as a whole (MSA total group, bars filled with gray); the latter shows neither unimodal (single peak) nor bimodal (double peak) curves. The upper histograms indicate the MSA group with glial cytoplasmic inclusions (GCIs) ($GCI^+$ group, bars filled with gray) or without GCIs ($GCI^-$ group, unfilled bars with black lines).

along the lines representing the normal distribution (Fig. 4). Although the control group exhibited a normal size distribution with a single peak, the data from the MSA total group (consisting of $GCI^+$ and $GCI^-$ groups) were not in a normal distribution. The nuclear volumes were significantly smaller in the MSA total group (135.81 ± 60.83 $\mu m^3$; mean ± SD; n = 404) compared with the control group (188.05 ± 55.71 $\mu m^3$; n = 308; $p < 0.001$ by the Mann-Whitney U test with Bonferroni correction). This difference was due to the significantly smaller nuclear volume of the $GCI^-$ group (91.26 ± 23.77 $\mu m^3$; n = 210) compared with the control group ($p < 0.001$ by 1-way ANOVA) and compared with the MSA $GCI^+$ group (184.03 ± 51.18 $\mu m^3$; n = 194; $p < 0.001$ by 1-way ANOVA). The nuclear volume of the $GCI^+$ group was not significantly different from that of the control group ($p > 0.05$ by 1-way ANOVA). Moreover, the nuclear volume of the $GCI^+$ group was significantly larger than that of the $GCI^-$ group ($p < 0.001$ by 1-way ANOVA). Thus, there was a selective decrease in nuclear volume that was restricted to the $GCI^-$ group.

## DISCUSSION

This is the first study to demonstrate a decrease in the actual nuclear volume of oligodendrocytes in the pons in MSA. This volume decrease was due to the smaller nuclear volume of $GCI^-$ than of the control, whereas the nuclear volume of $GCI^+$ was equivalent to that of the control. The technical novelty of this study includes 3D reconstruction of target structures (nuclei), followed by direct quantification of the entire structures.

Routine evaluation of histologic sections is usually performed on 2D basis on thin-sample specimens in which cell loss is perceived as a decrease in local density and atrophy as the volume loss of the cell body. One-dimensional indices such as diameter and perimeter are ready candidates for representing structure sizes, but sophisticated 2D indices such as cross-sectional area of the structures allow more precise determinations of their size. Using 2D quantification of neuronal size in the substantia nigra, Ma et al (19) demonstrated a 3.2% decrease per decade, whereas Cruz-Sánchez et al (20) reported progressive swelling with aging by simple comparisons of images. Similar discrepancies

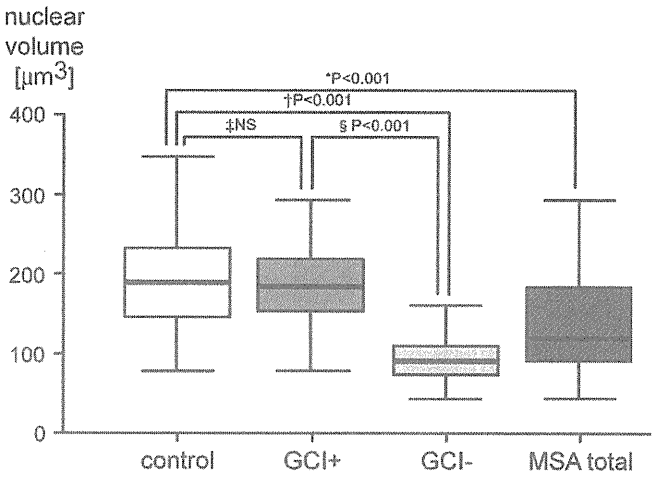


**FIGURE 3.** Comparison of size distribution of oligodendroglial nuclei from each group. Box plots show the nuclear volumes for each group (control; glial cytoplasmic inclusion $[GCI]^+$, oligodendrocytes with GCIs from multiple system atrophy [MSA] cases; $GCI^-$, oligodendrocytes without GCIs from MSA cases, MSA total, all oligodendrocytes from MSA cases). The boxes enclose the middle half of the values bounded by upper and lower quartiles. The bold lines represent the medians. The lower whisker indicates the smallest nonoutlier observation; the upper whisker indicates the nonoutlier observation. *, $p < 0.001$ when compared with control group (by the Mann-Whitney U test; Bonferroni correction); †, $p < 0.001$ when compared with control group (by 1-way analysis of variance [ANOVA]); ‡, NS, no significant difference when compared with control group (by 1-way ANOVA); §, $p < 0.001$ when compared with $GCI^+$ group (by 1-way ANOVA).

© 2009 American Association of Neuropathologists, Inc.



Copyright © 2009 by the American Association of Neuropathologists, Inc. Unauthorized reproduction of this article is prohibited.

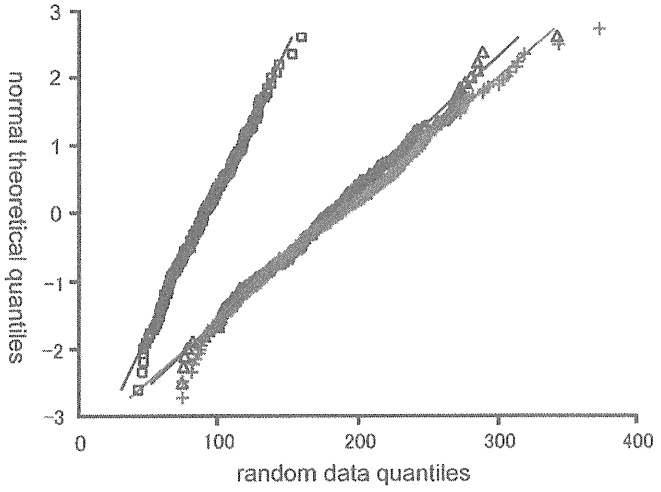


**FIGURE 4.** Normal distribution of nuclear volumes. The Q-Q plot shows the comparison of the distribution of a given variable with the normal distribution (represented by straight lines). The straight lines represent what the data would look like if they were normally distributed. The actual data are represented by the symbols plotted along this line; the closer the points are to the line, the more normally distributed the data appear. Most of the data points fall almost perfectly along the line, indicating that the data are normally distributed. Oligodendrocytes with glial cytoplasmic inclusions ($GCI^+$), open triangles; oligodendrocytes without GCIs ($GCI^-$) in multiple system atrophy (MSA), open squares; control, gray crosses. Q-Q, quantile-quantile.

among the studies have also been observed in Parkinson disease (21, 22), suggesting that 2D representation of 3D reality into a single plane is not sufficient.

Various stereologic methods have been developed by synthesizing 2D data sets to estimate volumes (10–12). These methods essentially include 2 steps: theoretically unbiased sampling of 2D raw data set and virtual estimation of the volume. Although still indirect, these innovative strategies made it possible to estimate the volume on a 3D basis. Even with these 3D quantification methods, however, Rudow et al (23) reported an age-associated increase of neuronal size on the substantia nigra using the nucleator method, whereas Cabello et al (24) demonstrated no decrease by using the rotator method; thus, there is similar disagreement as that generated using 2D studies. Because each of these groups was careful to ensure that the method of volume estimation used was unbiased, these conflicting results may be related to methodologic differences and their limitations.

Instead of using these indirect estimation methods, our direct method quantified the actual volume of nuclei reconstructed from serially obtained optical sections spanning the entire structure of oligodendrocytes, including the nucleus and GCIs when they were. To our knowledge, this is the first successful attempt to quantify directly the volume of pathologic structures in the human brain on a 3D basis. Because this strategy deals with the 3D reality and its direct measurement, it is completely free from bias that may derive from both sampling and estimation. The normal size distribution of the measured nuclear volumes in each case confirmed the reliability of our method of sampling and volumetry.

Using this method, we demonstrated that the nuclear volume of oligodendroglia in MSA is significantly smaller as a whole than in the control group, and that, although the nuclear volume of $GCI^+$ oligodendrocytes was equivalent to that of the control group, the $GCI^-$ oligodendrocytes are responsible for this volume reduction, that is, nuclear shrinkage seems to be accelerated in the absence of GCIs (Table 2).

Because the absence of significant differences among groups for age and sex might have been related to a limited number of cases with wide ranges of age at death (Table 1), statistical analyses were performed after omitting the youngest patient (Control 1; 47 years at death) to determine whether the exaggerated difference in age might give alternative results. Omission of Control 1 ($203.82 \pm 64.37$ $\mu m^3$; $n = 21$) did not result in a significant change in nuclear volume (new control group: $186.90 \pm 54.97$ $\mu m^3$; $n = 287$ vs entire control group, $188.05 \pm 55.71$ $\mu m^3$; $n = 308$, $p > 0.05$ or vs Control 1, $p > 0.05$ by Student *t*-test). This replicated the significant differences seen before the omission, that is, the $GCI^+$ group and the new control group are larger than the $GCI^-$ group ($p < 0.001$ by 1-way ANOVA), and the $GCI^+$ and the new control group are not significantly different ($p > 0.05$ by 1-way ANOVA). Although this study was not designed to identify age-related changes in the nuclear volume of oligodendrocytes, the size distributions of each group ($GCI^+$, $GCI^-$, and control) were compatible with the normal size distribution, suggesting that our sampling and volumetric procedures were appropriate to represent a single cell group corresponding to each category. Thus, it is clear that reduction of nuclear volume is evident exclusively in the $GCI^-$ group even if there were potentially confounding age-related changes.

It has been generally considered that the size/volume of the nuclei, nucleoli, and cell body of neurons undergo

**TABLE 3.** Three-Dimensional Volume Estimates and Their Changes in Relation to Aging and Degeneration

| | | Overall Change, % | Reference |
|---|---|---|---|
| Aging | SN neuron, $TH^+$* | +39 in SN neuron, +23 in $TH^+$ | 23 |
| | SN $m^+$ neuron† | No decrease | 24 |
| | NC neuron† | Decrease | 25 |
| PD | SN neuron* | Reduction | 23 |
| AD | ACG, PCG, CA1, PVC nucleolus, nuclei, neuron* | Hypertrophy in CA1/ACG of asymptomatic AD | 26 |
| ALS | MC nuclei, neuron† | No difference | 27 |
| TLE | TC neuron* | +28 in GM,+55 in WM | 28 |
| Alcoholics | Purkinje cell/nuclei, neuron† | −24 in cell body, −16 in nuclei | 29 |

*The nucleator method and its modifications.
†The rotator method and its modifications.
ACG, anterior cingulate gyrus; AD, Alzheimer disease; ALS, amyotrophic lateral sclerosis; CA1, Cornu ammonis 1; GM, gray matter; $m^+$, melanin-positive; MC, motor cortex; NC, neocortex; PCG, posterior cingulate gyrus; PD, Parkinson disease; PVC, primary visual cortex; SN, substantia nigra; TC, temporal cortex; $TH^+$, tyrosine hydroxylase–positive neuron; TLE, temporal lobe epilepsy; WM, white matter.


© 2009 American Association of Neuropathologists, Inc.

Copyright © 2009 by the American Association of Neuropathologists, Inc. Unauthorized reproduction of this article is prohibited.

shrinkage in aging and neurodegenerative processes. As expected, therefore, we demonstrated that the nuclear volumes of oligodendroglia in MSA cases as a whole are significantly reduced. Table 3 shows the summary of indirect 3D estimation of the volume of the nucleoli/nuclei/cell and their relation to aging and diseases; neurodegenerative processes are not necessarily related to volume reduction of neurons (26–28). Because these data were obtained without distinguishing the presence or absence of pathologic inclusions, however, how the disease-related changes identified are linked to pathologic inclusions is unclear. Indeed, several 2D morphometric studies have focused on the size of individual cells to identify cellular changes and their relationships to pathologic inclusions (Table 4). For example, transected nuclear areas of pontine neurons harboring nuclear inclusions are uniformly larger than those not harboring nuclear inclusions (32–34). Two-dimensional observations of a thin histologic plane may, however, not identify inclusions within the cell that are not present in the histologic plane. Our 3D reconstruction analysis spans the entire target structure, including pathologic inclusions, and therefore definitively determines whether or not pathologic inclusions are present. Although the relationships between disease-related changes and inclusion-related changes remain to be clarified, it is now possible to quantify 3D changes of each cell without bias after definitively determining the presence or absence of pathologic inclusions.

It is not surprising that the pathologic inclusions in MSA are related to a larger cell/nuclear size or a lesser extent of degeneration. There are similar examples in cell culture models (36, 37), transgenic animals (38, 39), and a variety of human conditions (30–35). It is not clear whether oligodendrocytes with and without GCI undergo completely different degenerative processes or whether they represent different aspects of a shared process. Because the distribution of the nuclear volume of MSA oligodendrocytes as a whole was neither unimodal (single peak) nor bimodal (double peaks; Fig. 2), it is likely that the $GCI^+$ and $GCI^-$ groups undergo some common mechanism of the degeneration. The selective decrease in nuclear volume restricted to the $GCI^-$ group cannot be explained if the nuclear shrinkage is accelerated in the presence of GCIs. Preserved nuclear volume of $GCI^+$ oligodendrocytes does not necessarily imply that they are free from the degenerative process.

Some studies have attempted to simulate the oligodendroglial pathology of MSA. For example, overexpression of human α-synuclein leads to the cytotoxicity in cultured oligodendrocytic progenitor cells (40), and transgenic mice that overexpress human wild-type α-synuclein show progressive locomotor dysfunction; histologic analyses showed the accumulation of detergent-insoluble α-synuclein similar to GCIs (41, 42) and system-oriented degeneration but with some differences from MSA (43, 44). Numerous studies of MSA patient brains have attempted to find possible correlations between GCIs and degeneration. In MSA, GCIs show a "system-oriented distribution in the suprasegmental motor systems (i.e. primary motor and higher motor areas of the cerebral cortex, pyramidal, extrapyramidal, and corticocerebellar systems) in the supraspinal autonomic systems and in their targets" (4), and changes in neurons follow a similar distribution pattern (2, 4, 6). Nevertheless, the density of GCIs and the severity of neuronal loss and their possible correlations claimed by previous studies are highly conflicting (2, 4, 6, 7, 45). Apoptosis-related proteins, including Bax (46) and activated caspase 3 (47), are reportedly present mainly in oligodendrocytes, often showing α-synuclein–positive inclusions (47). Interestingly, the cytoplasmic expression of Bcl-2, a putative anti-apoptotic protein, has been reported in oligodendrocytes with α-synuclein coexpression in approximately 25% of $GCI^+$ cells (46). Although the major question of whether GCIs are cytotoxic or cytoprotective remains to be answered, apoptosis with the morphologic feature of nuclear shrinkage (48) is considered to account for at least some of the oligodendroglial death in MSA (46, 47). In Parkinson disease and dementia with Lewy bodies (other degenerative processes with α-synuclein deposits [49, 50]), it is hypothesized that the aggregation of α-synuclein prevents or delays neuronal degeneration possibly by sequestering toxic protein species (51, 52). It remains to be determined whether a similar scenario may also explain the role of aggregation of α-synuclein as GCIs in MSA. The relative preservation of nuclear volume with GCI and accelerated shrinkage in the absence of GCIs in human brain are compatible with this possibility.

It is now possible to analyze the pathologic expression of specific molecules in relation to nuclear size. Molecular mechanisms bridging cellular/nuclear atrophy and GCI formation or other pathologic deposits are now candidate subjects for further study in a quantitative fashion rather than a "black and white" dualism such as neuronal death versus survival. The novel strategy for human brain studies used herein provides a pivotal viewpoint regarding the pathologic significance of GCIs and will be applicable to degenerative processes other than MSA.

TABLE 4. Two-Dimensional Area Quantification Studies and Their Dependence on Index Lesions

| | Target ± Index Lesion/Area | Change of Area Dependent on the Index Lesion, % | Reference |
|---|---|---|---|
| PD | SN neuron ± LBs/nucleolus, neuron | No difference | 30 |
| AD | Hippocampal neuron ± NFTs/nucleolus, neuron | No difference | 31 |
| MJD | Pontine neuron ± NAs/nucleus | −21% with NAs, −41% without NAs | 32 |
| NIID | Pontine neuron ± NIIs/nucleus | +22% with NIIs, −14% without NIIs | 33 |
| SCA1 | Pontine neuron ± NIs/nucleus | No difference with NIs, −12% without NIs | 34 |
| DRPLA | Cerebellar granule cell ± NIIs/nucleus | Larger with NIIs | 35 |

±, with/without; AD, Alzheimer disease; DRPLA, dentatorubral-pallidoluysian atrophy; LBs, Lewy bodies; MJD, Machado-Joseph disease; NA, nuclear aggregate; NFTs, neurofibrillary tangles; NI, nuclear inclusion; NII, neuronal intranuclear inclusion; NIID, neuronal intranuclear inclusion disease; PD, Parkinson disease; SCA1, spinocerebellar ataxia 1; SN, substantia nigra.

© 2009 American Association of Neuropathologists, Inc.



Copyright © 2009 by the American Association of Neuropathologists, Inc. Unauthorized reproduction of this article is prohibited.

## ACKNOWLEDGMENTS

*The authors thank Prof Hidekazu Tomimoto, MD, PhD, Department of Neurology, Mie University, Japan, and Hideaki Hayashi, MD, PhD, the former director of Tokyo Metropolitan Neurological Hospital, Japan, for their valuable help.*

## REFERENCES

1. Graham JG, Oppenheimer DR. Orthostatic hypotension and nicotine sensitivity in a case of multiple system atrophy. J Neurol Neurosurg Psychiatry 1969;32:28–34
2. Papp MI, Kahn JE, Lantos PL. Glial cytoplasmic inclusions in the CNS of patients with multiple system atrophy (striatonigral degeneration, olivopontocerebellar atrophy and Shy-Drager syndrome). J Neurol Sci 1989;94:79–100
3. Nakazato Y, Yamazaki H, Hirato J, et al. Oligodendroglial microtubular tangles in olivopontocerebellar atrophy. J Neuropathol Exp Neurol 1990; 49:521–30
4. Papp MI, Lantos PL. The distribution of oligodendroglial inclusions in multiple system atrophy and its relevance to clinical symptomatology. Brain 1994;117:235–43
5. Armstrong RA, Cairns NJ, Lantos PL. A quantitative study of the pathological changes in ten patients with multiple system atrophy (MSA). J Neural Transm 2004;111:485–95
6. Ozawa T, Paviour D, Quinn NP, et al. The spectrum of pathological involvement of the striatonigral and olivopontocerebellar systems in multiple system atrophy: Clinicopathological correlations. Brain 2004; 127:2657–71
7. Inoue M, Yagishita S, Ryo M, et al. The distribution and dynamic density of oligodendroglial cytoplasmic inclusions (GCIs) in multiple system atrophy: A correlation between the density of GCIs and the degree of involvement of striatonigral and olivopontocerebellar systems. Acta Neuropathol 1997;93:585–91
8. Mochizuki A, Mizusawa H, Ohkoshi N, et al. Argentophilic intracytoplasmic inclusions in multiple system atrophy. J Neurol 1992;239: 311–16
9. Abe H, Yagishita S, Amano N, et al. Argyrophilic glial intracytoplasmic inclusions in multiple system atrophy: Immunocytochemical and ultrastructural study. Acta Neuropathol 1992;84:273–77
10. Jensen EBV, Gundersen HJG. The rotator. J Microsc 1993;170:35–44
11. Gundersen HJG. The nucleator. J Microsc 1988;151:3–21
12. Gundersen HJG, Jensen EBV. The efficiency of systematic sampling in stereology and its prediction. J Microsc 1987;147:229–63
13. Rudin W. The Riemann-Stieltjes integral. In: Rudin W ed. *Principles of Mathematical Analysis*. 2nd ed. New York, NY: McGraw-Hill, 1964: 104–29
14. McNeal GR, Maynard WH, Branch RA, et al. Liver volume measurements and three-dimensional display from MR images. Radiology 1988; 169:851–54
15. Bakker J, Olree M, Kaatee R, et al. Renal volume measurements: Accuracy and repeatability of US compared with that of MR imaging. Radiology 1999;211:623–28
16. Kubínová L, Janácek J, Guilak F, et al. Comparison of several digital and stereological methods for estimating surface area and volume of cells studied by confocal microscopy. Cytometry 1999;36:85–95
17. Kanazawa T, Uchihara T, Takahashi A, et al. Three-layered structure shared between Lewy bodies and Lewy neurites-three-dimensional reconstruction of triple-labeled sections. Brain Pathol 2008;18:415–22
18. Suzuki M, Raisman G. The glial framework of central white matter tracts: Segmented rows of contiguous interfascicular oligodendrocytes and solitary astrocytes give rise to a continuous meshwork of transverse and longitudinal processes in the adult rat fimbria. Glia 1992;6: 222–35
19. Ma SY, Röytt M, Collan Y, et al. Unbiased morphometrical measurements show loss of pigmented nigral neurones with ageing. Neuropathol Appl Neurobiol 1999;25:394–99
20. Cruz-Sánchez FF, Cardozo A, Tolosa E. Neuronal changes in the substantia nigra with aging: A Golgi study. J Neuropathol Exp Neurol 1995;54:74–81
21. Neal JW, Pearson RC, Cole G, et al. Neuronal hypertrophy in the pars reticulata of the substantia nigra in Parkinson's disease. Neuropathol Appl Neurobiol 1991;17:203–6
22. Ma SY, Rinne JO, Collan Y, et al. A quantitative morphometrical study of neuron degeneration in the substantia nigra in Parkinson's disease. J Neurol Sci 1996;140:40–45
23. Rudow G, O'Brien R, Savonenko AV, et al. Morphometry of the human substantia nigra in ageing and Parkinson's disease. Acta Neuropathol 2008;115:461–70
24. Cabello CR, Thune JJ, Pakkenberg H, et al. Ageing of substantia nigra in humans: Cell loss may be compensated by hypertrophy. Neuropathol Appl Neurobiol 2002;28:283–91
25. Stark AK, Toft MH, Pakkenberg H, et al. The effect of age and gender on the volume and size distribution of neocortical neurons. Neuroscience 2007;150:121–30
26. Iacono D, O'Brien R, Resnick SM, et al. Neuronal hypertrophy in asymptomatic Alzheimer disease. J Neuropathol Exp Neurol 2008;67: 578–89
27. Toft MH, Gredal O, Pakkenberg B. The size distribution of neurons in the motor cortex in amyotrophic lateral sclerosis. J Anat 2005;207: 399–407
28. Bothwell S, Meredith GE, Phillips J, et al. Neuronal hypertrophy in the neocortex of patients with temporal lobe epilepsy. J Neurosci 2001;21: 4789–800
29. Andersen BB. Reduction of Purkinje cell volume in cerebellum of alcoholics. Brain Res 2004;1007:10–18
30. Gertz HJ, Siegers A, Kuchinke J. Stability of cell size and nucleolar size in Lewy body containing neurons of substantia nigra in Parkinson's disease. Brain Res 1994;637:339–41
31. Gertz HJ, Schoknecht G, Krüger H, et al. Stability of cell size and nucleolar size in tangle-bearing neurons of the hippocampus in Alzheimer's disease. Brain Res 1989;487:373–75
32. Uchihara T, Iwabuchi K, Funata N, et al. Attenuated nuclear shrinkage in neurons with nuclear aggregates-a morphometric study on pontine neurons of Machado-Joseph disease brains. Exp Neurol 2002;178: 124–28
33. Uchihara T, Tanaka J, Funata N, et al. Influences of intranuclear inclusion on nuclear size—Morphometric study on pontine neurons of neuronal intranuclear inclusion disease cases. Acta Neuropathol 2003; 105:103–8
34. Nagaoka U, Uchihara T, Iwabuchi K, et al. Attenuated nuclear shrinkage in neurones with nuclear inclusions of SCA1 brains. J Neurol Neurosurg Psychiatry 2003;74:597–601
35. Takahashi H, Egawa S, Piao YS, et al. Neuronal nuclear alterations in dentatorubral-pallidoluysian atrophy: Ultrastructural and morphometric studies of the cerebellar granule cells. Brain Res 2001;919:12–19
36. Saudou F, Finkbeiner S, Devys D, et al. Huntingtin acts in the nucleus to induce apoptosis but death does not correlate with the formation of intranuclear inclusions. Cell 1998;95:55–66
37. Arrasate M, Mitra S, Schweitzer ES, et al. Inclusion body formation reduces levels of mutant huntingtin and the risk of neuronal death. Nature 2004;431:805–10
38. Yamamoto A, Lucas JJ, Hen R. Reversal of neuropathology and motor dysfunction in a conditional model of Huntington's disease. Cell 2000; 101:57–66
39. Klement IA, Skinner PJ, Kaytor MD, et al. Ataxin-1 nuclear localization and aggregation: role in polyglutamine-induced disease in SCA1 transgenic mice. Cell 1998;95:41–53
40. Tsuboi K, Grzesiak JJ, Bouvet M, et al. Alpha-synuclein overexpression in oligodendrocytic cells results in impaired adhesion to fibronectin and cell death. Mol Cell Neurosci 2005;29:259–68
41. Yazawa I, Giasson BI, Sasaki R, et al. Mouse model of multiple system atrophy α-synuclein expression in oligodendrocytes causes glial and neuronal degeneration. Neuron 2005;45:847–59
42. Kahle PJ, Neumann M, Ozmen L, et al. Hyperphosphorylation and insolubility of α-synuclein in transgenic mouse oligodendrocytes. EMBO Rep 2002;3:583–88
43. Shults CW, Rockenstein E, Crews L, et al. Neurological and neurodegenerative alterations in a transgenic mouse model expressing human α-synuclein under oligodendrocyte promoter: Implications for multiple system atrophy. J Neurosci 2005;25:10689–99
44. Stefanova N, Reindl M, Neumann M, et al. Oxidative stress in transgenic mice with oligodendroglial α-synuclein overexpression replicates the

 © 2009 American Association of Neuropathologists, Inc.

Copyright © 2009 by the American Association of Neuropathologists, Inc. Unauthorized reproduction of this article is prohibited.

characteristic neuropathology of multiple system atrophy. Am J Pathol 2005;166:869–76
45. Sakamoto M, Uchihara T, Nakamura A, et al. Progressive accumulation of ubiquitin and disappearance of α-synuclein epitope in multiple system atrophy-associated glial cytoplasmic inclusions: Triple fluorescence study combined with Gallyas-Braak method. Acta Neuropathol 2005;110:417–25
46. Probst-Cousin S, Rickert CH, Schmid KW, et al. Cell death mechanisms in multiple system atrophy. J Neuropathol Exp Neurol 1998;57: 814–21
47. Jellinger KA, Stadelmann CH. The enigma of cell death in neurodegenerative disorders. J Neural Transm Suppl 2000;(60):21–36
48. Kerr JF, Wyllie AH, Currie AR. Apoptosis: A basic biological phenomenon with wide-ranging implications in tissue kinetics. Br J Cancer 1972;26:239–57
49. Spillantini MG, Schmidt ML, Lee VM, et al. α-Synuclein in Lewy bodies. Nature 1997;388:839–40
50. Tu PH, Galvin JE, Baba M, et al. Glial cytoplasmic inclusions in white matter oligodendrocytes of multiple system atrophy brains contain insoluble α-synuclein. Ann Neurol 1998;44:415–22
51. McNaught KS, Shashidharan P, Perl DP, et al. Aggresome-related biogenesis of Lewy bodies. Eur J Neurosci 2002;16:2136–48
52. Johnston JA, Ward CL, Kopito RR. Aggresomes: A cellular response to misfolded proteins. J Cell Biol 1998;143:1883–98

© 2009 American Association of Neuropathologists, Inc.



Copyright © 2009 by the American Association of Neuropathologists, Inc. Unauthorized reproduction of this article is prohibited.

Biochemical and Biophysical Research Communications xxx (2009) xxx–xxx

Contents lists available at ScienceDirect

Biochemical and Biophysical Research Communications

journal homepage: www.elsevier.com/locate/ybbrc

# Dopamine facilitates α-synuclein oligomerization in human neuroblastoma SH-SY5Y cells

Kentaro Yamakawa [a], Yasuhiko Izumi [b], Hiroki Takeuchi [c], Noriyuki Yamamoto [b], Toshiaki Kume [b], Akinori Akaike [b], Ryosuke Takahashi [c], Shun Shimohama [c,d], Hideyuki Sawada [a,*]

[a] Clinical Research Center, Utano National Hospital, National Hospital Organization, Kyoto 616-8255, Japan
[b] Department of Pharmacology, Graduate School of Pharmaceutical Sciences, Kyoto University, Kyoto, Japan
[c] Department of Neurology, Graduate School of Medicine, Kyoto University, Kyoto, Japan
[d] Department of Neurology, School of Medicine, Sapporo Medical University, Hokkaido, Japan

ARTICLE INFO

*Article history:*
Received 29 October 2009
Available online xxxx

*Keywords:*
α-Synuclein
Oligomer
Aggregation
Dopamine
Size exclusion chromatography
Parkinson's disease

ABSTRACT

Parkinson's disease is characterized by selective loss of dopaminergic neurons in the substantia nigra and by the appearance of Lewy bodies. Fibrillar α-synuclein is the main component of Lewy bodies. Previous studies have suggested that dopamine promotes α-synuclein oligomerization and that partially aggregated or oligomeric α-synuclein could be cytotoxic. To confirm this hypothesis using cell cultures, we performed size exclusion chromatography as a pretreatment method prior to Western blotting to more clearly detect a small amount of α-synuclein oligomers in wild-type α-synuclein-overexpressing SH-SY5Y cells. Using this method, we confirmed that stable overexpression of α-synuclein in SH-SY5Y cells indeed increased the amounts of α-synuclein oligomers in these cells and exposure of the cells to dopamine for 6 h facilitated α-synuclein oligomerization. These dopamine-induced α-synuclein oligomers continued to exist for the following 24 h. However, the dopamine-treated cells did not undergo cell death or apoptosis in spite of the presence of increased oligomeric α-synuclein. Our data may contribute to the understanding of the mechanisms underlying α-synuclein oligomer formation and its suspected cytotoxicity toward dopaminergic neurons.

© 2009 Elsevier Inc. All rights reserved.

## Introduction

Parkinson's disease (PD) is among the most prevalent neurodegenerative disorders. It is characterized by selective loss of dopaminergic neurons in the mesencephalic substantia nigra and by the presence of cytoplasmic inclusions, namely Lewy bodies.

One of the key molecules involved in the pathogenesis of PD is α-synuclein, the major component of Lewy bodies. α-Synuclein is a 140-amino acid protein, which exists predominantly in presynaptic nerve terminals in the brain [1,2]. Physiologically, it adopts a soluble, unfolded structure [3]; however, in the pathological state, it is supposed to aggregate and form fibrillar deposits within Lewy bodies [4].

Mutations [E46K, A53T], duplication or triplication of the α-synuclein gene increase the propensity of α-synuclein to aggregate and are linked to autosomal-dominant-inherited PD [4]. These findings again imply that aggregation and accumulation of α-synuclein are critical in the pathogenesis of PD. α-Synuclein polymerizes from soluble monomers, to dimers, trimers or oligomers, eventually becoming fibrillar aggregates. It has been hypothesized that, among these aggregated α-synuclein species, α-synuclein oligomers might be toxic to cells [5].

Previous studies have shown that dopamine promotes aggregation of monomeric α-synuclein and stabilizes oligomeric species of α-synuclein both in cell-free systems [6,7] and cultured cells [8,9]. However, in cultured cells, it is technically difficult to detect α-synuclein oligomers only by Western blotting (WB), especially when these are of wild-type α-synuclein. The purpose of this study was to determine whether dopamine promotes wild-type α-synuclein aggregation and whether aggregated α-synuclein has cytotoxicity in cultured cells. Because wild-type α-synuclein exists mainly as a soluble monomer in cells, and the amount of α-synuclein oligomers is thought to be far less than the amount of monomer, we separated cell lysates by size exclusion chromatography (SEC) prior to WB to differentiate α-synuclein oligomers from monomers. Using this method, we studied the interactions between dopamine and α-synuclein aggregation and cytotoxicity in human dopaminergic neuroblastoma SH-SY5Y cells.

## Materials and methods

*Materials.* α-Synuclein, GBR 12935, anti-α-tubulin antibody and protease inhibitor cocktail (P8340) were purchased from Sigma

* Corresponding author. Fax: +81 75 464 0027.
*E-mail address:* sawada@unh.hosp.go.jp (H. Sawada).

0006-291X/$ - see front matter © 2009 Elsevier Inc. All rights reserved.
doi:10.1016/j.bbrc.2009.11.015

Please cite this article in press as: K. Yamakawa et al., Dopamine facilitates α-synuclein oligomerization in human neuroblastoma SH-SY5Y cells, Biochem. Biophys. Res. Commun. (2009), doi:10.1016/j.bbrc.2009.11.015

(St. Louis, MO). Dopamine hydrochloride was purchased from Nacalai Tesque (Kyoto, Japan). Gel filtration standards were purchased from Bio-Rad (Hercules, CA). Rabbit polyclonal anti-α-synuclein antibody was purchased from Santa Cruz Biotechnology (sc-7011R, Santa Cruz, CA). Anti-cleaved caspase-3 antibody (Cell Signaling Technology, Beverly, MA) was used to detect caspase-3 activation. The lactate dehydrogenase (LDH) release assay was carried out using the Cytotoxicity Detection LDH kit from Kyokuto Pharmaceutical Industrial (Tokyo, Japan).

*Plasmid construction.* Plasmid construction was performed as previously reported [10]. α-Synuclein cDNA was amplified from postmortem human brain samples by RT-PCR using *Kpn*I- and *Xba*I-tailed primers complementary to the human α-synuclein coding region (GenBank AY049786). The nucleotide sequences of sense and antisense primers were as follows: 5′-CGGGGTACCTG GCCATTCGACGACAGTGT-3′ (sense), 5′-TGCTCTAGAGGATGGAACAT CTGTCAGCA-3′ (antisense). Appropriate restriction digestion of the PCR-amplified product was performed and the wild-type sequence was then cloned into the pcDNA3.1(+) vector (Invitrogen, San Diego, CA). Plasmid DNA was subsequently transformed into DH5α cells (Toyobo, Osaka, Japan). The resulting colonies were screened by PCR, and positives were selected, grown in liquid medium, and sequenced to verify the wild-type α-synuclein sequence (data not shown).

*Stable transfection.* The human dopaminergic neuroblastoma cell line SH-SY5Y was maintained at 37 °C in a humidified atmosphere of 5% $CO_2$ in Dulbecco's modified Eagle's medium supplemented with 10% fetal bovine serum, 2 mM glutamine, 100 U/mL penicillin, and 100 μg/mL streptomycin. When cells reached 80% confluency in 60-mm culture dishes, the medium was changed to Opti-MEM I (Invitrogen) and cells were transfected with 8 μg of wild-type α-synuclein DNA constructs using 10 μg of Lipofectamine 2000 (Invitrogen). After incubating the cells for 24 h, positive clones were selected using G418 (1300 μg/mL) for 2 weeks. Single cells were cloned in 96-well tissue culture plates. Stable transfectants established from these clones were evaluated for α-synuclein expression using Western blot analysis and immunocytochemistry.

*Cell culture.* SH-SY5Y cells were maintained in Opti-MEM I supplemented with 10% fetal bovine serum and incubated at 37 °C in a humidified atmosphere of 95% air and 5% $CO_2$. Cells were seeded in 24-well culture plates for the LDH release assay, or in 100-mm dishes for WB or SEC. Cells were grown for 72 h and then exposed to drugs.

*LDH release assay for determination of viability of SH-SY5Y cells.* The viability of SH-SY5Y cells was determined by LDH release assay, as described previously [11]. The activity of LDH released into the medium during the exposure to drugs was measured using a LDH assay kit. Aliquots (25 μL) of culture supernatants were mixed with 75 μL of the LDH substrate mixture contained in the assay kit. After incubation for 1 h at room temperature, the reaction was stopped by adding 100 μL of 1 N hydrochloride (HCl) and the absorbance was measured at 570 nm. LDH release from the cultured cells was evaluated as a percentage of the total LDH released following exposure to 1 mM hydrogen peroxide for 24 h.

*HPLC-ED analysis of dopamine.* Dopamine concentrations were measured by high-performance liquid chromatography with electrochemical detection (HPLC-ED). SH-SY5Y cells were washed twice with cold phosphate-buffered saline (PBS) and scraped in 1 mL of PBS. Cells were then centrifuged at 5000 rpm for 5 min, and homogenized in 300 μL of solubilizing buffer (0.1 N perchloric acid, 10 mM sodium disulfite, 1 mM ethylene diamine tetraacetic acid–disodium salt (EDTA–2Na) by sonication. After centrifugation at 15,000*g* for 15 min at 4 °C, the supernatants were collected for HPLC. Aliquots (10 μL) of the supernatants were analyzed by HPLC-ED. The HPLC system (HTEC-500, Eicom, Kyoto, Japan) consisted of a pump, a degasser, a column oven and an electrochemical detector with a graphite working electrode. The working electrode was maintained at an oxidative potential of +450 mV vs. an Ag/AgCl reference electrode to detect dopamine. The separation of dopamine from other endogenous compounds was achieved on a reversed-phase column (Eicompak CA-5ODS, Eicom) using a mixture of 0.1 M phosphate buffer (pH 6.0) and methanol (88:12, v/v) containing 600 mg/L sodium 1-octanesulfonate and 50 mg/L EDTA–2Na as a mobile phase. The column temperature was kept at 25 °C and the mobile phase was delivered at a flow rate of 0.23 mL/min.

*Size exclusion chromatography and subsequent Western blotting.* SH-SY5Y cells were washed twice with cold PBS and scraped in 1 mL of PBS. Cells were then centrifuged at 5000 rpm for 5 min, and homogenized in PBS by sonication. After centrifugation at 15,000*g* for 30 min at 4 °C, supernatants were filtered through a 0.2 μm hydrophilic PTFE disposable membrane (Millex-LG, Millipore). Protein concentrations were determined using Bradford's assay (Bio-Rad) and some amounts (2000–3000 μg) was loaded onto Shodex SEC columns (Showa Denko, Tokyo, Japan). The columns were equilibrated with mobile phase buffer (0.01 M Tris–HCl, pH 7.0, 0.15 M NaCl and 0.2% N-lauroylsarcosine) before analysis. Samples were eluted at a flow rate of 0.25 mL/min, and fractions were collected 1 mL per tube. The absorbance value at OD 280 nm of each fraction was used to draw the elution profile. For WB, equal volumes (10 μL) of each fraction were mixed with 2× sample buffer (0.125 M Tris–HCl, 20% glycerol, 4% sodium dodecyl sulfate (SDS), bromophenol blue), without boiling, loaded onto a 5–20% polyacrylamide gradient gel (e-PAGEL, ATTO, Tokyo, Japan) for SDS–polyacrylamide gel electrophoresis (SDS–PAGE) and transferred to polyvinylidene difluoride (PVDF) membranes (Immobilon-$P^{SQ}$, Millipore). The membranes were then incubated in 5% dry milk in Tris-buffered saline with Tween 20 (TBS-T, 20 mM Tris, 137 mM NaCl, 0.1% Tween 20, pH 7.6) at room temperature for 1 h and incubated with α-synuclein antibodies (1:1000 dilution) in blocking solution (3% bovine serum albumin, 0.05% sodium azide in PBS) overnight at 4 °C. The membranes were then washed four times, 10 min each, in TBS-T, followed by 1 h incubation in horse radish peroxidase (HRP) conjugated secondary antibody (1:2000 dilution). The membranes were next washed six times, 10 min each, in TBS-T before incubation in chemiluminescence reagents (ECl plus, GE Healthcare) and then exposed to film. All procedures were performed on ice.

The SEC system consisted of a system controller (SCL-$10A_{VP}$, Shimadzu, Kyoto, Japan), a degasser (DGU-14A, Shimadzu), a solvent delivery (LC-$10AT_{VP}$, Shimadzu), an auto-sampler (SIL-$10AD_{VP}$, Shimadzu), a column oven (CTO-$10AC_{VP}$, Shimadzu), a guard column (KW-G; Showa Denko), Shodex silica-based columns (KW-802.5, KW-803, Showa Denko), a photodiode array detector (SPD-$M10A_{VP}$, Shimadzu), a fraction collector (FRC-10A, Shimadzu) and a sample cooler. For better separation, three silica-based columns were lineated (from the upper side, KW-803, KW-803, and KW-802.5 in this sequence). Data acquisition and processing were carried out using Class VP software (Shimadzu). The SEC conditions were as follows: injection volume 500 μL (including 2000–3000 μg of protein), flow rate 0.25 mL/min, column temperature 25 °C, sample cooler temperature 4 °C.

*Western blotting for cleaved caspase-3.* SH-SY5Y cells were harvested as described above and homogenized in lysis buffer (0.02 M Tris, pH 7.0, 25 mM β-glycerophosphate, 2 mM EGTA, 1% Triton X-100, with a 1% protease inhibitor cocktail) by sonication. After centrifugation at 15,000*g* for 30 min at 4 °C, supernatants were collected and protein concentrations were determined. Twenty micrograms of each sample was mixed with 2× sample buffer (0.125 M Tris–HCl, 20% glycerol, 4% SDS, 31 mg/mL dithiothreitol, bromophenol blue), boiled for 5 min, loaded on a 5–20% polyacrylamide gradient gel for SDS–PAGE and transferred to PVDF

Please cite this article in press as: K. Yamakawa et al., Dopamine facilitates α-synuclein oligomerization in human neuroblastoma SH-SY5Y cells, Biochem. Biophys. Res. Commun. (2009), doi:10.1016/j.bbrc.2009.11.015

membranes. The membranes were incubated with anti-cleaved caspase-3 antibody (1:1000 dilution) and appropriate HRP-conjugated secondary antibodies (1:2000 dilution). Immunoreactive proteins on membranes were visualized with ECl plus.

*Statistical analysis.* The statistical significance of the differences among three or more groups of individual data was analyzed by one-way analysis of variance (ANOVA) and a post hoc multiple comparison using Dunnett's test. Statistical significance was defined as $P < 0.05$. Data are expressed as means ± SEM.

## Results

### *Detection of α-synuclein oligomers by size exclusion chromatography and subsequent Western blotting*

The silica-based columns used here gave linear elution profiles of a set of protein standards having molecular weights of 1.35–670 kDa, indicating efficient column separation (Fig. 1A). The elution profiles of wild-type α-synuclein-overexpressing SH-SY5Y cells for monomeric and oligomeric α-synuclein are shown in Fig. 1B. α-Synuclein monomer, dimer, trimer, and tetramer bands were detected mainly in fractions 27, 25, 24, and 23, respectively (Fig. 1B). Monomeric bands were also detected in these oligomers fractions, suggesting that SDS dissolved the oligomeric α-synuclein to monomer. A higher molecular weight smear was also detected (Fig. 1B). By contrast, the elution profiles of untransfected cells showed smaller amounts of endogenous α-synuclein monomer with only slightly detectable oligomer bands (Fig. 1C).

### *Dopamine facilitated α-synuclein oligomerization and its effect is suppressed by a DAT inhibitor*

Next we examined the effect of dopamine on α-synuclein oligomerization in wild-type α-synuclein-overexpressing SH-SY5Y cells. To this end, we first investigated the cellular content of dopamine when cells were exposed to dopamine. Wild-type α-synuclein-overexpressing cells were exposed to 100 μM dopamine for 45 min in the presence or absence of 3.2 μM GBR 12935, a dopamine transporter (DAT) inhibitor. Dopamine concentrations in cell lysates were measured by HPLC. While no detectable amount of dopamine was found in untreated cells, it was detected in dopamine-treated cells (Fig. 2A). In addition, co-administration of 3.2 μM GBR 12935 with dopamine significantly reduced the cellular content of dopamine, indicating that extracellular dopamine was taken up by cells via the dopamine transporter. We examined the elution profiles of dopamine-treated cells for α-synuclein. Wild-type α-synuclein-overexpressing cells were incubated in the presence or absence of 100 μM dopamine for 6 h and cell lysates were separated by SEC. To compare the subtle difference in the amount of α-synuclein oligomer, equal volumes (10 μL) of fractions 19–25 of sham- and dopamine-treated samples were analyzed by SDS–PAGE in a single 5–20% gradient gel, and immunoblotted for α-synuclein. When the elution profiles of dopamine-treated cell lysates (Fig. 2B, right half of the gel) were compared with that of sham treatment (Fig. 2B, left half of the gel), the intensities of oligomeric α-synuclein bands in fractions 21–23 were apparently increased (Fig. 2B and C). Furthermore, the intensities of monomeric α-synuclein bands in fraction 21–23 were also slightly increased (Fig. 2B, right half of the gel), indicating that a portion of dopamine-induced oligomers was denatured by SDS (Fig. 2B and C). These changes, however, could not be detected when the same samples were immunoblotted without SEC, suggesting that SEC worked as an efficient pretreatment method before WB to detect small amounts of dopamine-induced α-synuclein oligomers (Fig. 2D). When the cells were co-treated with dopamine and GBR 12935, the increase in the amount of α-synuclein oligomers was suppressed (Fig. 2E). Overall, these findings suggested that dopamine was taken up by the dopamine trans-

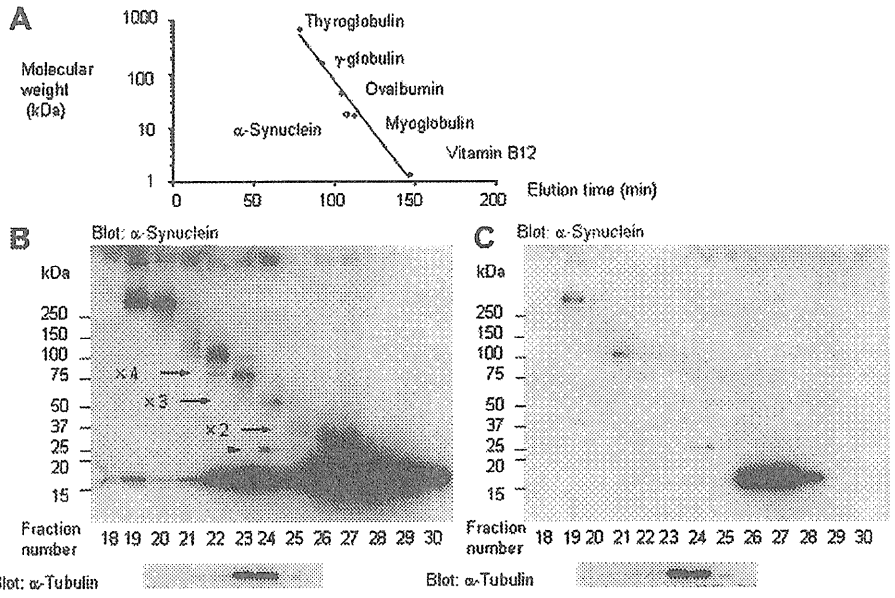


**Fig. 1.** Elution profiles of SEC (A) and detection of α-synuclein oligomers in SH-SY5Y cells (B, C). (A) Calibration curve for SEC. The linearity of the calibration curve indicates efficient column separation. Protein size markers and molecular weights are as follows: thyroglobulin (670 kDa), γ-globulin (158 kDa), ovalbumin (44 kDa), myoglobin (17 kDa), and vitamin B12 (1.35 kDa) (filled circles). Recombinant monomeric α-synuclein (18 kDa) is shown as an open circle. (B, C) Detection of α-synuclein oligomeric bands in SH-SY5Y cells. Equal amounts (2000 μg of protein) of the PBS-soluble cell lysates were separated by SEC and 10 μL of each collected fraction was analyzed by SDS–PAGE in 5–20% gradient gels. The PVDF blots were analyzed for α-synuclein (upper panel) and re-blotted for α-tubulin as a loading control (lower panel). (B) Cell lysates from wild-type α-synuclein-overexpressing SH-SY5Y cells were analyzed. Films were exposed for long enough to detect trace oligomeric bands, so the monomeric α-synuclein bands were saturated. α-Synuclein dimer, trimer, and tetramer were detected (arrow). The 25-kDa band in fraction 24 (arrowhead) was a non-specific band. Higher molecular species were also detected. (C) Cell lysates from untransfected SH-SY5Y cells were analyzed. The film exposure time was the same as in (B). Note, endogenous α-synuclein monomer was detected in fraction 27.

Please cite this article in press as: K. Yamakawa et al., Dopamine facilitates α-synuclein oligomerization in human neuroblastoma SH-SY5Y cells, Biochem. Biophys. Res. Commun. (2009), doi:10.1016/j.bbrc.2009.11.015

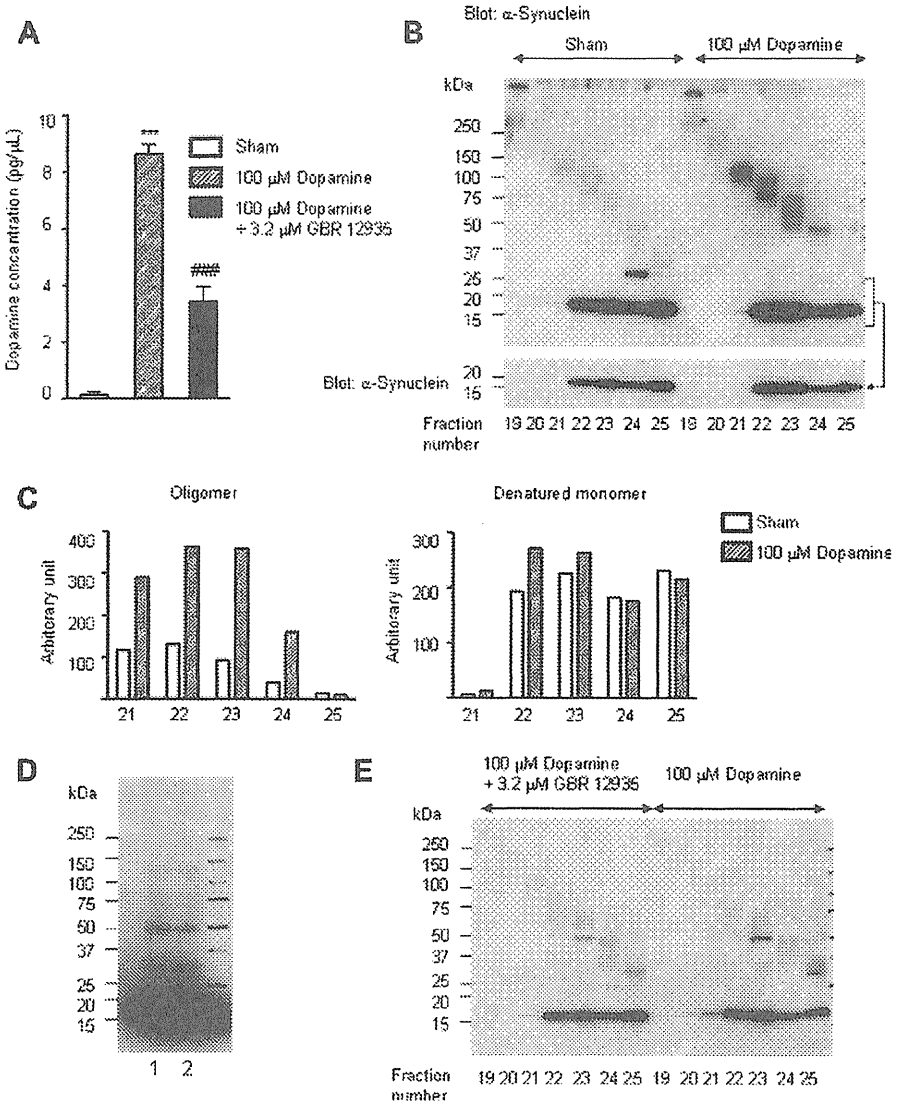


**Fig. 2.** Dopamine content (A) and α-synuclein oligomerization (B–E) after dopamine treatment. (A) Intracellular uptake of dopamine via the dopamine transporter. Wild-type α-synuclein-overexpressing SH-SY5Y cells were exposed to 100 μM dopamine for 45 min in the presence or absence of GBR 12935. Cells were collected in PBS and homogenized in 300 μL of solubilizing buffer. After centrifugation at 15,000*g* for 15 min at 4 °C, supernatants were analyzed for dopamine content by HPLC. $^{***}P < 0.001$ compared with sham treatment. $^{\#\#\#}P < 0.001$ compared with dopamine alone. $n = 3$ dish/experiment. Data were expressed as means ± SEM. (B) Dopamine facilitated α-synuclein oligomerization in wild-type α-synuclein-overexpressing SH-SY5Y cells. Cells were exposed to 100 μM dopamine for 6 h and equal amounts (3000 μg of protein) of cell lysate from the PBS-soluble fraction were separated by SEC. Ten-microliter aliquots of each of fractions 19–25 from sham and dopamine treatments were analyzed by SDS–PAGE in a single 5–20% gradient gel. The PVDF blots were analyzed for α-synuclein. Compared with sham treatment (left half of the gel), the amounts of α-synuclein oligomers were increased by dopamine treatment (right half of the gel). Lower panel shows monomeric α-synuclein bands with the film exposed for a shorter time than in the upper panel. The results are representative of three independent experiments. (C) The blots shown in (B) were quantified using NIH ImageJ software for the relative amounts of α-synuclein oligomers and their denatured monomers. White bars represent sham treatment. Striped bars represent dopamine treatment. (D) The same samples as shown in (B), before SEC, were analyzed by WB for α-synuclein. Lane 1, sham treatment. Lane 2, 100 μM dopamine treatment for 6 h. WB without SEC could not detect any difference in the amount of α-synuclein oligomer. (E) When cells were exposed to dopamine in the presence of GBR 12935, formation of α-synuclein was suppressed. Cells were exposed to 100 μM dopamine with or without 3.2 μM GBR 12935 for 6 h, and same amount (2000 μg of protein) of PBS-soluble cell lysate was separated by SEC. Ten-microliter aliquots of each of fractions 19–25 from dopamine-treated cells, with or without GBR 12935, were analyzed by SDS–PAGE in the same 5–20% gradient gel. The PVDF blots were stained for α-synuclein. Compared with dopamine treatment alone (right half of the gel), the amounts of α-synuclein oligomers were decreased by dopamine treatment with 3.2 μM GBR 12935 (left half of the gel).

porter and facilitated wild-type α-synuclein oligomerization in cells.

### *α-Synuclein oligomer continued to exist in cells up to 24 h after washing out dopamine-containing medium but did not cause cell death*

Because it has been hypothesized that α-synuclein oligomers are cytotoxic, we investigated the effect of dopamine-induced α-synuclein oligomers on cell viability. To this end, wild-type α-synuclein-overexpressing SH-SY5Y cells were exposed to 100 μM dopamine for 6 h and incubated in dopamine-free medium for a further 24 h. The elution profile of dopamine washout treatment showed that almost the same amount of α-synuclein oligomer was still found in the cells after 24 h of washout time, compared with no washout treatment (Fig. 3A). An LDH release assay revealed that cells were viable after 24 h washout time (Fig. 3B). In addition, though staurosporine-induced apoptotic cells

Please cite this article in press as: K. Yamakawa et al., Dopamine facilitates α-synuclein oligomerization in human neuroblastoma SH-SY5Y cells, Biochem. Biophys. Res. Commun. (2009), doi:10.1016/j.bbrc.2009.11.015

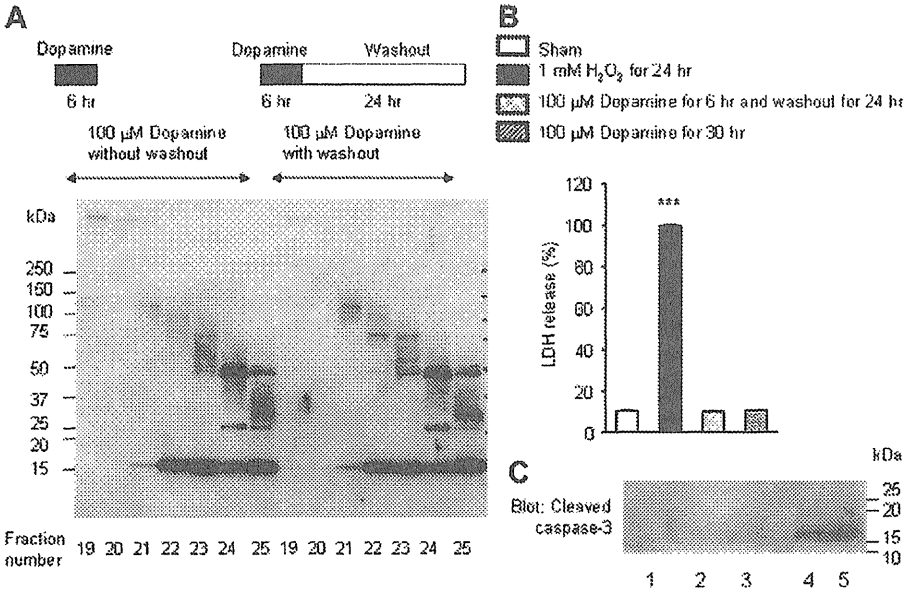


**Fig. 3.** Twenty-four hours-persistent oligomers in cells and their cytotoxicity (A–C). (A) Dopamine-induced α-synuclein oligomers existed in cells after removal of dopamine from the medium for 24 h. α-Synuclein-overexpressing SH-SY5Y cells were exposed to 100 μM dopamine for 6 h. After that, cells were incubated in dopamine-free medium for a further 24 h. The same amount (2000 μg of protein) of cell lysate was separated by SEC and 10 μL aliquots of each of fractions 19–25 from dopamine-treated cells with or without 24 h washout treatment were analyzed for α-synuclein. Almost the same amount of α-synuclein oligomer still existed after removal of dopamine for 24 h (right half of the gel), compared with dopamine treatment for 6 h (left half of the gel). (B) An LDH assay showed that the dopamine-treated cells with oligomeric α-synuclein did not undergo cell death within the following 24 h. Wild-type α-synuclein-overexpressing SH-SY5Y cells were exposed to 100 μM dopamine for 6 h. After that, the cells were incubated in dopamine-free medium for further 24 h. No difference in LDH release was found between sham treatment and dopamine treatment. $^{***}P < 0.001$ compared with sham treatment. $n = 4$ dish/experiment. Data were expressed as means ± SEM. (C) Caspase-3 was not activated in dopamine-treated cells with oligomeric α-synuclein. α-Synuclein-overexpressing SH-SY5Y cells were treated with dopamine or staurosporine and analyzed by WB for cleaved caspase-3. Cleaved caspase-3 levels did not increase following dopamine treatment. Lane 1, control. Lane 2, treatment with 100 μM dopamine for 6 h. Lane 3, treatment with 100 μM dopamine for 6 h with 24 h washout time. Lane 4, treatment with 0.25 μM staurosporine for 3 h. Lane 5, treatment with 0.25 μM staurosporine for 6 h.

caused cleavage of caspase-3, this was not observed in dopamine-treated cells (Fig. 3C). These findings suggested that neither cell death nor apoptosis had occurred, in spite of the fact that α-synuclein oligomers still existed in the cells.

## Discussion

In this study, we adopted the combined methods of SEC and WB to detect wild-type α-synuclein oligomers in cells. Although we could not distinguish α-synuclein oligomers from α-synuclein bound to other proteins, their molecular weights and sequential separation by SEC suggested that these bands with oligomeric molecular weights included α-synuclein oligomers. Previous studies have analyzed cell lysates of α-synuclein-overexpressing cells by combining SEC and WB [8,12]; however, only monomeric wild-type α-synuclein bands, but not oligomeric bands, were detected in these studies. In our study, oligomeric α-synuclein bands themselves, especially tetramers were detected. It is said that in most cell models the recovered α-synuclein is predominantly monomeric on SDS–PAGE gels [13]. We suspect that this might reflect, in part, the nature of α-synuclein oligomers that are sensitive to SDS or heating. Therefore, in this study, the non-boiling sample preparation condition may have helped make the detection of α-synuclein oligomer bands easier. Another means of detecting oligomeric α-synuclein is delipidation treatment. Sharon et al. [14] reported that α-synuclein oligomers could also be detected by simple WB with non-boiled samples (from mouse brains) when heat was added to blotted PVDF membranes or samples were delipidated, and therefore, that some α-synuclein oligomers were not detected by WB because they were bound to lipid in cells. Therefore, lipid-bound α-synuclein was not detected in this study.

Exposure of α-synuclein-overexpressing cells to dopamine promoted oligomerization of α-synuclein. These data were consistent with the findings of previous studies using recombinant α-synuclein [6,7] or cultured cells [8,9]. They reveal that dopamine promotes the formation of SDS-resistant α-synuclein oligomers within 5 min [7] to 3 days [6] in a cell-free system or within 3–5 days [8,9] in cells. We demonstrated that intracellular oligomerization was facilitated by dopamine within 6 h, and that the oligomers were stable for at least 24 h.

A previous study using A53T mutant- and tyrosine hydroxylase mutant-overexpressing SH-SY5Y cells revealed that α-synuclein oligomers were innocuous [8]. These results are consistent with our study. However, it has been controversial whether over-expressed α-synuclein, some part of which may be oligomerized as shown in Fig. 2, is cytotoxic or innocuous [13]. Therefore, the cytotoxicity of oligomeric α-synuclein requires confirmation in further experiments.

In conclusion, we demonstrated that dopamine promotes wild-type α-synuclein oligomerization in cells and that these α-synuclein oligomers did not cause cytotoxicity, at least up to 24 h. Further study is needed to elucidate the relationship between α-synuclein oligomerization and Parkinson's disease.

## References

[1] R. Jakes, M.G. Spillantini, M. Goedert, Identification of two distinct synucleins from human brain, FEBS Lett. 345 (1994) 27–32.
[2] A. Iwai, E. Masliah, M. Yoshimoto, N. Ge, L. Flanagan, H.A. de Silva, A. Kittel, T. Saitoh, The precursor protein of non-A beta component of Alzheimer's disease amyloid is a presynaptic protein of the central nervous system, Neuron 14 (1995) 467–475.
[3] P.H. Weinreb, W. Zhen, A.W. Poon, K.A. Conway, P.T. Lansbury Jr., NACP, a protein implicated in Alzheimer's disease and learning, is natively unfolded, Biochemistry 35 (1996) 13709–13715.

Please cite this article in press as: K. Yamakawa et al., Dopamine facilitates α-synuclein oligomerization in human neuroblastoma SH-SY5Y cells, Biochem. Biophys. Res. Commun. (2009), doi:10.1016/j.bbrc.2009.11.015

ARTICLE IN PRESS



[4] E.A. Waxman, B.I. Giasson, Molecular mechanisms of alpha-synuclein neurodegeneration, Biochim. Biophys. Acta 1792 (2009) 616–624.
[5] M.J. Volles, P.T. Lansbury Jr., Zeroing in on the pathogenic form of alpha-synuclein and its mechanism of neurotoxicity in Parkinson's disease, Biochemistry 42 (2003) 7871–7878.
[6] K.A. Conway, J.C. Rochet, R.M. Bieganski, P.T. Lansbury Jr., Kinetic stabilization of the alpha-synuclein protofibril by a dopamine-alpha-synuclein adduct, Science 294 (2001) 1346–1349.
[7] R. Cappai, S.L. Leck, D.J. Tew, N.A. Williamson, D.P. Smith, D. Galatis, R.A. Sharples, C.C. Curtain, F.E. Ali, R.A. Cherny, J.G. Culvenor, S.P. Bottomley, C.L. Masters, K.J. Barnham, A.F. Hill, Dopamine promotes alpha-synuclein aggregation into SDS-resistant soluble oligomers via a distinct folding pathway, FASEB J. 19 (2005) 1377–1379.
[8] J.R. Mazzulli, A.J. Mishizen, B.I. Giasson, D.R. Lynch, S.A. Thomas, A. Nakashima, T. Nagatsu, A. Ota, H. Ischiropoulos, Cytosolic catechols inhibit alpha-synuclein aggregation and facilitate the formation of intracellular soluble oligomeric intermediates, J. Neurosci. 26 (2006) 10068–10078.
[9] C.E. Moussa, F. Mahmoodian, Y. Tomita, A. Sidhu, Dopamine differentially induces aggregation of A53T mutant and wild type alpha-synuclein: insights into the protein chemistry of Parkinson's disease, Biochem. Biophys. Res. Commun. 365 (2008) 833–839.
[10] R. Kohno, H. Sawada, Y. Kawamoto, K. Uemura, H. Shibasaki, S. Shimohama, BDNF is induced by wild-type alpha-synuclein but not by the two mutants, A30P or A53T, in glioma cell line, Biochem. Biophys. Res. Commun. 318 (2004) 113–118.
[11] Y. Izumi, H. Sawada, N. Sakka, N. Yamamoto, T. Kume, H. Katsuki, S. Shimohama, A. Akaike, *p*-Quinone mediates 6-hydroxydopamine-induced dopaminergic neuronal death and ferrous iron accelerates the conversion of *p*-quinone into melanin extracellularly, J. Neurosci. Res. 79 (2005) 849–860.
[12] J. Xu, S.Y. Kao, F.J. Lee, W. Song, L.W. Jin, B.A. Yankner, Dopamine-dependent neurotoxicity of alpha-synuclein: a mechanism for selective neurodegeneration in Parkinson disease, Nat. Med. 8 (2002) 600–606.
[13] M.R. Cookson, M. van der Brug, Cell systems and the toxic mechanism(s) of alpha-synuclein, Exp. Neurol. 209 (2008) 5–11.
[14] R. Sharon, I. Bar-Joseph, M.P. Frosch, D.M. Walsh, J.A. Hamilton, D.J. Selkoe, The formation of highly soluble oligomers of alpha-synuclein is regulated by fatty acids and enhanced in Parkinson's disease, Neuron 37 (2003) 583–595.

Please cite this article in press as: K. Yamakawa et al., Dopamine facilitates α-synuclein oligomerization in human neuroblastoma SH-SY5Y cells, Biochem. Biophys. Res. Commun. (2009), doi:10.1016/j.bbrc.2009.11.015

*Epilepsia*, **(*):1–4, 2009
doi: 10.1111/j.1528-1167.2009.02309.x

BRIEF COMMUNICATION

# Mutations in *LGI1* gene in Japanese families with autosomal dominant lateral temporal lobe epilepsy: The first report from Asian families

*Jun Kawamata, *Akio Ikeda, *Youshi Fujita, †[1]Keiko Usui, *[2]Shun Shimohama, and *Ryosuke Takahashi

*Department of Neurology and †Human Brain Research Center, Kyoto University Graduate School of Medicine, Shogoin, Sakyo-ku, Kyoto, Japan

## Summary

**Autosomal dominant lateral temporal lobe epilepsy (ADLTE) caused by *LGI1* (leucine-rich gene, glioma-inactivated-1) mutations is a rare familial epileptic syndrome characterized by the auditory ictal manifestation and rare nocturnal generalized seizures. We have examined the sequence of the *LGI1* gene in four Japanese families with lateral temporal lobe epilepsy having characteristic auditory features, and identified one novel (1421G>A), and one reported (1418C>T) point mutation each in two families. These two mutations were 3 bp apart in the *LGI1* gene and caused adjoining amino acid substitutions. The two families presented different clinical phenotypes and seizure control to drug treatment. These findings suggest that *LGI1* mutations in Japanese ADLTE families may not be uncommon, and that diverse clinical phenotypes make adequate diagnosis of ADLTE difficult when only based on clinical information.**

**KEY WORDS: ADLTE, *LGI1*, Mutation, Psychiatric symptoms, Panic attack–like symptoms.**

Autosomal dominant lateral temporal lobe epilepsy (ADLTE, MIM 600512) is a rare form of lateral temporal lobe epilepsy with characteristic manifestations such as auditory and visual auras, seizures triggered by auditory stimuli, and rare nocturnal generalized seizures (Gu et al., 2005). The majority of hereditary idiopathic epileptic disorders are caused by mutations of genes encoding ion channel components. The only exception in human so far is ADLTE, which is caused by mutations in *LGI1*, leucine-rich glioma inactivated-1, a gene encoding a secreted neuronal protein (Fukata et al., 2006).

In 1995, the linkage analysis of a large family with partial epilepsy showed strong evidence for localization of a gene for partial epilepsy on 10q22-24 (Ottman et al., 1995). In 2002 the *LGI1* was identified as a causative gene, and its mutations in five families with ADLTE were reported (Kalachikov et al., 2002). To date more than 13 point mutations with amino acid substitutions and one insertion, five deletions, three point mutations resulting in premature truncations, and one point mutation resulting in skipping two exons have been reported (Morante-Redolat et al., 2002; Fertig et al., 2003; Gu et al., 2005; Chabrol et al., 2007). No pathologic polymorphism was found in the promoter region of *LGI1* (Bovo et al., 2008). Clinical semiology seems to vary among families, but no analyses with regard to the different ethnics were done because of absence of reports of ADLTE from Asian countries. Herein we report the first, non-Caucasian ADLTE families with *LGI1* mutations. The content of this article has not appeared elsewhere except for in abstract form (Ikeda et al., 2007).

Accepted July 24, 2009; Early View publication Xxxx xx, 2009.

Address correspondence to Akio Ikeda, M.D., Ph.D., Department of Neurology, Kyoto University Graduate School of Medicine, 54 Shogoin-Kawaharacho, Sakyo-ku, Kyoto 606-8507, Japan. E-mail: akio@kuhp.kyoto-u.ac.jp

Present addresses: [1]National Epilepsy Center, Shizuoka Institute of Epilepsy and Neurological Disorders, Shizuoka, Japan.

[2]Department of Neurology, Sapporo Medical University School of Medicine, Sapporo, Hokkaido, Japan.

Wiley Periodicals, Inc.
© 2009 International League Against Epilepsy

## Subjects and Methods

### Subjects

In 2005 and 2006, we had four families who were clinically consistent with a diagnosis of ADLTE. They were treated for their seizure disorders at Kyoto University Hospital and resided in Kyoto province. Two families of four carried different heterozygous mutations in the *LGI1* gene,